Department of Physics and Astronomy
University of Heidelberg

Master thesis
in Physics
submitted by

Lilo Höcker

born in Baden (CH)

2019

Building up a modular Na-K quantum gas experiment

This Master thesis has been carried out by Lilo Höcker

at the

Kirchhoff Institute of Physics

under the supervision of

Jun.-Prof. Dr. Fred Jendrzejewski

ABSTRACT

Building up a modular Na-K quantum gas experiment

This thesis describes the construction of a second generation, ultracold atomic mixture experiment, aiming for modularity, robustness and compactness. The setup is designed to work with Bose-Fermi (^{23}Na,^{40}K) and Bose-Bose (^{23}Na,^{39}K) mixtures. The experimental setup consists of two separate two-dimensional magneto-optical traps (2D-MOTs) which pre-cool the atoms to efficiently load them into the dual-species three-dimensional magneto-optical trap (3D-MOT). This serves as a source of cold atoms for further steps of the experiment. During the course of this thesis, the mobile vacuum system as well as the laser system was built up for both species, culminating in the recent observation of a sodium 3D-MOT.

Aufbau eines modularen Na-K Quantengas Experiments

Diese Arbeit beschreibt den Aufbau eines modularen, robusten und kompakten ultra-kalten Atomgemisch-Experiments der 2. Generation. Der Aufbau ist so konzipiert, dass sowohl Bose-Fermi (^{23}Na, ^{40}K) als auch Bose-Bose (^{23}Na,^{39}K) Gemische untersucht werden können. Der experimentelle Aufbau besteht aus zwei getrennten zwei-dimensionalen magneto-optische Fallen (2D-MOTs), die die Atome vorkühlen um diese effizient in die gemeinsame drei-dimensionale magneto-optische Falle (3D-MOT) zu laden. Diese dient als Quelle kalter Atome für die weiteren Schritte des Experiments. Im Laufe dieser Arbeit wurden sowohl das mobile Vakuumsystem als auch das Lasersystem für beide Arten aufgebaut, was jüngst zur Beobachtung einer Natrium 3D-MOT führte.

CONTENTS

LIST OF FIGURES

MOTIVATION

The characteristics of ultracold atomic experiments are the precise control of experimental parameters, such as interaction strength, temperature, or dimensionality. Therefore, ultracold quantum systems can be employed as simulators for physical processes, which are governed by analogous equations [1, 2], and thus enabling the possibility to study different physical systems in a controlled and tunable way. The control of the interaction strength between two species in an ultracold atomic mixture, enhances the possibilities even further. This thesis describes the steps taken so far, to build up a second generation mixture experiment within our group, emphasising design decisions. The old experiment, which uses lithium and sodium, faces instabilities, which are caused among other reasons by the complexity of the system. With the new experiment, we are aiming at a modular, robust, and compact setup that can be operated 24/7, being stable enough to run through several experimental cycles.

Considering the wealth of available literature and the exciting experiences in the *matterwave* group, we chose sodium and potassium as atomic species, since a certain simplification of the experimental implementation and robustness of the setup is expected. Especially potassium with its natural isotopes ^{39}K and ^{40}K gives the modularity to switch between bose-bose and bose-fermi mixtures, increasing the possible physical systems to study. Another advantage of this pair of species are the moderately wide inter-species Feshbach resonances below $300\,\mathrm{G}$, that provide easy tunability of inter-species interactions [3, 4].

With the new experiment we would like to study among others the following physical processes:

QUANTUM THERMODYNAMICS

Not all atomic species can be sufficiently cooled with optical methods. Inter-species interactions can be used to sympathetically cool neutral atoms using atoms of another species [5–7]. Alternatively, the quantum analogue of a refrigerator offers a new approach for a cooling scheme [8]. In this approach, two bosonic atomic clouds (red and blue in fig. 1.1) e. g. of Na, are coupled by a tightly confined fermionic cloud e. g. ^{40}K. The fermionic cloud acts as a working fluid and can be used to transfer energy from the cold (blue) Na cloud to the hot (red) one in each refrigeration cycle. The external laser compensates the necessary work input. The sodium cloud should be cooled below the condensation

threshold, over the course of many cycles. The refrigeration cycle (Otto cycle) is illustrated in figure 1.1.
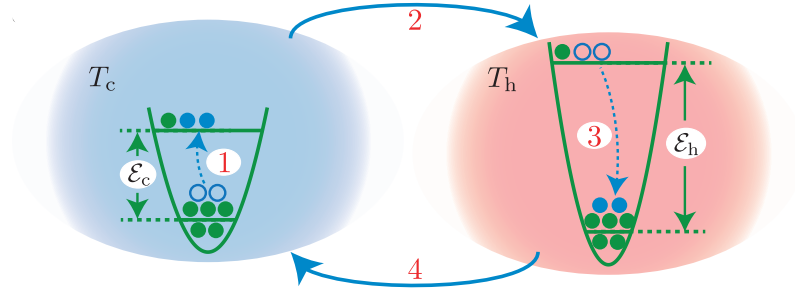
Figure 1.1: Quantised Otto cycle. The strongly confined ^{40}K cloud which acts as working medium (green), is transferred between the hot (red) and cold (blue) ^{23}Na baths. (1,3) Thermalisation of the working medium with a cold (hot) bath. (2,4) Adiabatic change of the energy level spacings of the working fluid. Figure taken from [8].

CONDENSED MATTER PHYSICS

[9] The Kondo effect describes the temperature dependence of the electric conductivity in metals. At a characteristic temperature T_K a conductivity minimum occurs in alloys. A magnetic impurity of spin $S = 1/2$ interacts with metal hosts of non-interacting fermions with spins of $s = 1/2$ (fig. 1.2). For temperatures above T_K, the system is well described by a fermi liquid (fig. 1.2 c). The fermions weakly scatter on the impurity. For intermediate temperatures, the impurity is bound into a many-body singlet ground state, giving rise to polarisation of the impurity due to fermions hopping into the impurity region, leading to interactions between the fermions (fig. 1.2 b). For temperatures below T_K, the impurity gets screened by the Kondo screening cloud, due to the confinement in the many-body singlet ground state. Surrounding fermions scatter on the impurity region and can, therefore, be described as a fermi liquid (fig. 1.2 a). The Kondo screening cloud is of high interest [10]. Consequently, ultracold atomic physics could be used to study the Kondo screening cloud and its dynamics. This system can be experimentally realised with a ^{23}Na impurity immersed in a Fermi sea of ^{40}K atoms [11].

HIGH ENERGY PHYSICS

Gauge fields are of high interest to particle physics, since they cause strong and electro-weak forces between matter. Studying gauge fields in the original system is difficult for both experimental and theoretical approaches, due to the complex many-body dynamics [12, 13]. In the

a) Fermi Liquid   b) Strong Coupling Regime   c) Fermi Liquid

$$T \ll T_K \qquad\qquad T_K \qquad\qquad T \gg T_K$$
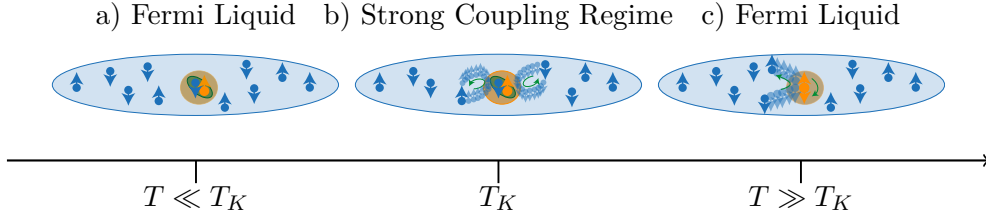
Figure 1.2: Demonstrating the interaction between fermions $s = 1/2$ and a magnetic impurity $S = 1/2$ at different temperatures. a) For temperatures far below T_K the impurity is confined in a many-body singlet ground state, and therefore screened by a so called Kondo screening cloud. The fermions are described as a Fermi liquid. b) At T_K the impurity is in the many-body singlet ground state, however, fermions can enter the region and polarise the impurity. Due to the polarization, the fermions interact with each other, resulting in a strong coupling. c) Well above T_K the fermions scatter weakly on the impurity and can be described as fermi liquid. Figure taken from [9].

standard model of high energy physics, elementary particles are divided into matter particles (fermions), which can sit on a lattice, and gauge bosons, which are responsible for the interactions, and thus described as link [14, 15]. Lattice gauge theories can be implemented in an atomic experiment, using Bose-Fermi mixtures on a tilted lattice. Spin-changing collisions are used to implement gauge-invariant couplings [16].
The thesis is structured in the following way:

Chapter 2 gives a review on the theoretical background of trapping and cooling of atoms.

Chapter 3 describes the setup of the vacuum system, to create the appropriate environment for the experiment.

Chapter 4 is dedicated to the laser system, where light is generated, stabilised and shifted to the desired frequencies.

Chapter 5 describes the pre-cooling of the atoms in a two dimensional magneto-optical trap (2D-MOT).

Chapter 6 describes the setup for the three dimensional magneto-optical trap considering the constraints of further experimental features to implement.

2

REVIEW: TRAPPING AND COOLING

Before discussing our experimental setup for cooling and trapping (chapter 5 and chapter 6), a short review on the theoretical concepts is given. This chapter mainly follows C.J. Foot Atomic Physics, 2005 [17].

2.1 ATOM-LIGHT INTERACTION

Consider a two-level atom with velocity V in a light field of photons with momentum $\hbar k$ (fig. 2.1 a). The atom can get excited by absorbing a photon, which transfers its momentum $\hbar k$ to the atom (fig. 2.1 b). After a while, the atom decays back to its ground state via spontaneous emission. The emitted photon is not restricted to any direction, so that on average the scattering of photons slows down the atom (figure 2.1 c).

a) Atom in light field b) Absorption c) Spontaneous emission
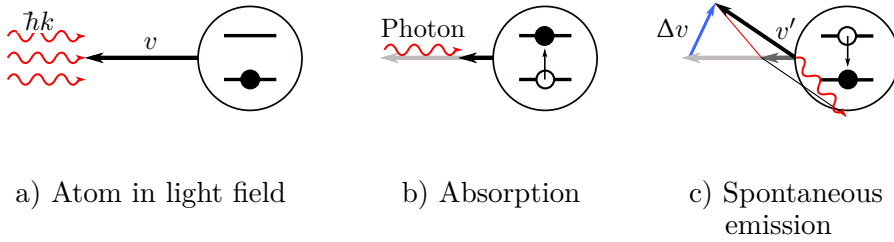
Figure 2.1: (a) Consider an atom moving with velocity v in the opposite direction to the light field. (b) The atom can absorb a photon of the light field. This excites the atom and reduces the atom's velocity. (c) Due to spontaneous emission, the atom relaxes to the ground state, while a photon is emitted in a random direction. This leads to a change in the atom's velocity.[18]

The resulting scattering force can be written as

$$F_{scatt} = \hbar k \frac{\Gamma}{2} \frac{I/I_{\mathrm{SAT}}}{1 + I/I_{\mathrm{SAT}} + 4\delta^2/\Gamma^2} \quad , \tag{2.1}$$

with photon momentum $\hbar k$, spontaneous emission rate Γ, detuning δ, intensity I and saturation intensity I_{SAT}. For high intensities the scattering force saturates to a limiting value

$$F_{scatt,max} = \frac{\hbar k \Gamma}{2} \quad , \tag{2.2}$$

where the factor $\frac{1}{2}$ indicates an average population of the excited state of $\frac{1}{2}$.[17]

2.2   LASER COOLING

This scattering force can be used to cool down atoms efficiently. The discovery of these techniques was acknowledged with the 1997 Nobel prize (Steven Chu [19], Claude Cohen-Tannoudji [20] and William Phillips [21]).

2.2.1   *Slowing an Atomic Beam*

Shining a laser against a counter-propagating atomic beam is not sufficient to cool the atoms. Due to the Doppler effect, the resonance frequency depends on the velocity of the atoms. The beam would therefore only slow down atoms, which have a certain velocity being resonant with the laser light. After having been slightly slowed down, the atoms are not resonant any more and are therefore not further cooled. In order to cool the atoms significantly, the frequency of the laser has to be adjusted according to the velocity of the atoms (Chirp Cooling). However, changing the frequency of the laser precisely is not so easy. Another possibility requires applying a magnetic field, which varies along the atoms propagation direction, so that atomic levels are shifted by the Zeeman effect (Zeeman Slower). The further the atoms travel against the light field, the lower is their velocity, as demonstrated in figure 2.2.[22],[17]
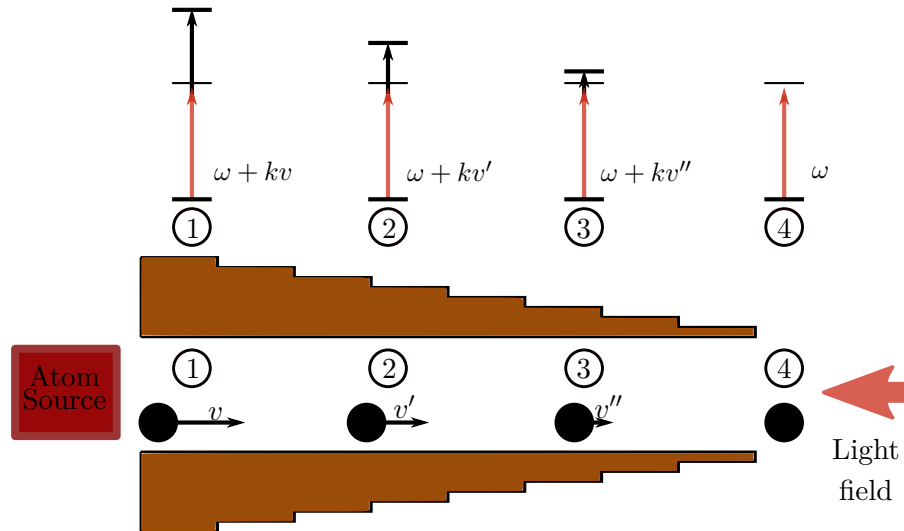
Figure 2.2: Atoms created by an atomic source are slowed down with a magnetic field decreasing with distance from the oven, and a counter propagating light field (Zeeman Slower). (1) Atomic source emits atoms with velocity v. Due to the magnetic field the excited state is shifted, such that the Doppler-shifted laser is resonant with the transition. (2) The magnetic field has to be reduced, since the atom's velocity decreased to v'. (3) The atom's velocity reduced to v'', therefore, a small magnetic field is sufficient to shift the levels. (4) The laser is not resonant with atoms with $v = 0$, thus they are not effected.

2.2.2 *Optical Molasses*

The scattering force can also be used to slow down atoms in all three spatial dimensions using counter-propagating beams, as sketched in figure 2.3 a. The forces resulting from the counter-propagating beams cancel each other out for stationary atoms, whereas moving atoms will experience a force imbalance due to the Doppler effect, as illustrated in figure 2.3 b.
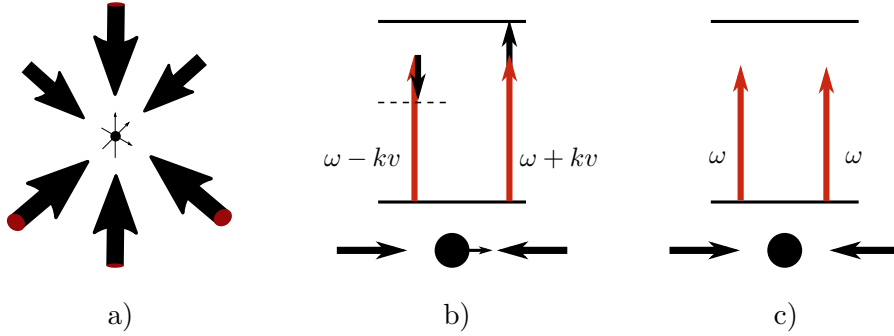
Figure 2.3: Optical molasses slows atoms down in all three dimensions. (a) To create an optical molasses three red-detuned beams and their counter-propagating beams are needed. (b) An atom moving with velocity v, for which the Doppler shift just compensates the detuning of one laser beam, will absorb the light and, therefore, slow down. The laser beam pointing in the same direction than the atom's velocity does not affect the atom, since it is not resonant. (c) For an atom with $v = 0$ both beams are red detuned and do not affect the atom. [17]

The total force can be written as

$$F_{molasses} = F_{scatt}(\omega - \omega_0 - kv) - F_{scatt}(\omega - \omega_0 + kv) \qquad (2.3)$$

$$\simeq -2\frac{\partial F}{\partial \omega}kv \qquad (2.4)$$

where low velocities $kv \ll \Gamma$ have been assumed. The force can be written in the form

$$F_{molasses} = -\alpha v \qquad (2.5)$$

which has the form of a frictional or damping force, since it always opposes the atoms velocity. For intensities well below saturation, the damping coefficient α can be written as

$$\alpha = 4\hbar k^2 \frac{I}{I_{SAT}} \frac{-2\delta/\Gamma}{[1 + (2\delta/\Gamma)^2]^2}. \qquad (2.6)$$

Since the damping coefficient has to be positive, the detuning δ has to be negative for the force to be frictional.

The temperature that can be achieved with this technique is limited by random recoil kicks due to spontaneous emission. The Doppler cooling limit for a detuning of $\delta = -\Gamma/2$ is given by

$$k_B T_D = \frac{\hbar\Gamma}{2}. \tag{2.7}$$

2.2.3 *Magneto Optical Trapping*

The optical molasses technique cools down atoms, that accumulate near the intersection of the laser beams. It is possible to trap the atoms using an additional magnetic field gradient and circularly polarised laser beams. A typical setup is shown in figure 2.4a. In this configuration, atoms are slowed down due to the velocity dependent force induced by the red-detuned laser, as we have seen it in the optical molasses case. In additionally to this, the atoms are trapped by a spatially dependent force induced by the magnetic field gradient. The magnetic sub-levels split depending on the position z, as shown in figure 2.4b (one dimension). In positive z-direction the magnetic field is positive, thus, the σ_- light is resonant with the transition, for negative z the σ_+ light is resonant. This results in a force imbalance, pushing the atoms towards the trap centre. [17]

(a) MOT setup

(b) MOT mechanism for $J = 0$ to $J = 1$ transition.
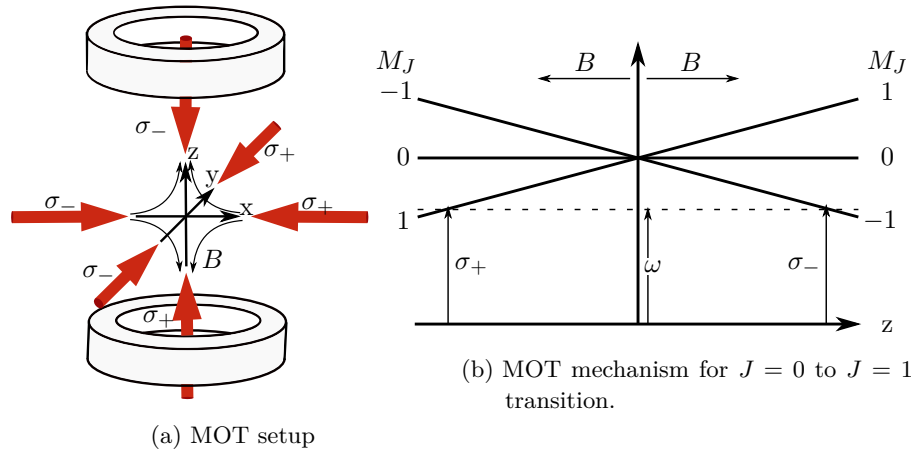
Figure 2.4: Magneto optical trap (MOT). (a) For a MOT three orthogonal red-detuned beams and their counter propagating beams are needed. Each beam pair consists of σ_- and σ_+ polarisation. In addition to this, a magnetic field gradient is needed, which is typically produced by gradient-field Maxwell coils. The quadrupole magnetic field lines in the $x - z$ plane is indicated by arrows. (b) Consider the 1D-case along the z-axis. The red-detuned laser does not affect an atom sitting in the trap centre. However, if an atom moves away from the centre, an imbalance of scattering forces pushes the atom back to the centre. [17]

2.2.4 *Multilevel Atoms*

So far, we have limited the discussion to two-level atoms. Although the two-level atom is a nice and simple model to explain the basic principles, reality is more complicated [23]. Taking multilevel structure into account, it is also possible that the atoms relax into a different state, where the chosen cooling frequency is not resonant. In order not to loose these atoms another frequency is chosen, the so-called repumper, to pump those atoms back.

Atoms can have degenerate sub-levels, where the transitions are polarisation-dependent. Therefore, it is possible to get below the Doppler cooling limit with the optical molasses technique. Two counter-propagating laser beams with orthogonal linear polarisation create a polarisation gradient, which results in position-dependent energies of these sub-ground states. An atom that is moving in the standing wave, loses kinetic energy by climbing the potential hill. It is then optically pumped, via an excited state, into the valley of the other ground state, where it starts to climb the potential hill again (figure 2.5). In analogy to Greek mythology this process is known as Sisyphus cooling. This only works for a small velocity regime. [17, 24]
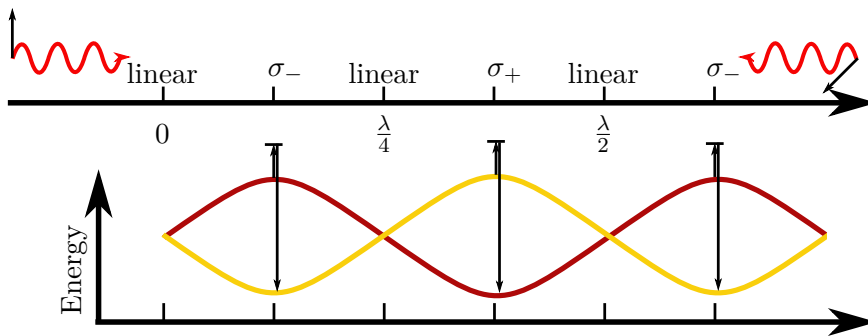
Figure 2.5: Two counter-propagating waves with orthogonal polarisations result in a polarisation gradient, depending on the distance and their relative phase. Considering an atom with initially two degenerate ground states (red and yellow), the energy of these ground states depends now on position. An atom moving along the standing wave, starting in the red ground state, converts kinetic energy into potential energy and then gets optically pumped into the yellow ground state. This cycle of energy conversion and optical pumping is repeated multiple times resulting in a reduction of kinetic energy and therefore cooling. [17]

2.3 SUMMARY

In this chapter we have described how to slow down and trap atoms using red-detuned laser light and magnetic fields. For the described concepts two-level atoms have been assumed. With Alkalis as multi-

level atoms with degenerated sub-levels, we expect a lower cooling limit than the Doppler cooling limit, but also need a repumper so that atoms aren't lost in states where the cooling light has no effect.

VACUUM

Ultra-cold experiments require atoms at low temperatures (nK). Since atoms transfer kinetic energy and heat up when they collide, the mean free path has to be increased. The mean free path is sufficiently large in an ultra-high vacuum (UHV) at pressures smaller than 10^{-11} mbar. In this chapter the vacuum setup is introduced, emphasising on design choices. Experimental techniques required to achieve a UHV vacuum are described as well.

Vacuum is classified in different pressure regions: Rough vacuum, high vacuum (HV), and ultra high vacuum (UHV) [25]. An overview of the different pressure regions is given in figure 3.1.
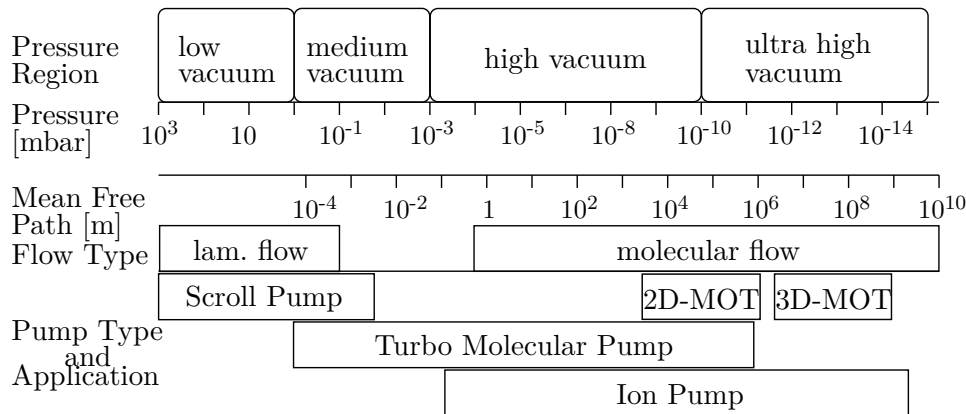
Figure 3.1: Different vacuum regions and the corresponding mean free path. The operating pressure ranges for our pumps and applications are indicated below. Figure adopted from [25]

In order to achieve a UHV, a series of different pumps is needed to get from one vacuum region to another (more details in section 3.2). Pumping alone is not sufficient as a proper sealing has to be ensured. There are standardised flanges and corresponding sealing on the market. Klein Flanges (KF) with an O-ring sealing, can be used up to the high vacuum region. For UHV applications copper sealing and ConFlat (CF) flanges are typically used. The CF flanges have a cutting edge, which cuts into the soft copper. While the O-rings can be used multiple times, a copper sealing can only be used once, due to the plastic deformation. For non-standardised flange, i. e. a flange without cutting-edge, sealings have to be done manually. Indium wire is often used, due to its good deformation and welding properties. [25]

3.1 VACUUM SETUP

Designing the vacuum chamber, the following requirements should be taken into account:

- `Optical Access:` The science chamber needs enough optical access for the three-dimensional magneto-optical trap (3D-MOT), imaging and dipole beams.

- `Material of Chambers:` The material used for manufacturing the vacuum chambers should have low out-gassing rates and be non-magnetic due to the atoms magnetic sensitivity.[26]

- `Slow down Atoms:` In the atoms need to be slowed down, in order to be trapped. This is usually achieved either by a Zeeman slower or a 2D-MOT. [27]

- `Standardised Sealing:` Ideally, the chambers are designed in a way that one uses standardised flanges and sealings, to simplify assembly.

In order to make the system as modular as possible, the following additional requirements are set:

- `Separation of Species:` A separated atom source and a pre-cooling region for each species makes it easy to switch between the two species. Moreover, this has the advantage that one does not have to compromise when setting the parameters for this stage of cooling e. g. the oven temperature.

- `Translation Stage:` Mounting the vacuum system on a translation stage makes it possible to move the system away from the 3D-MOT optics and coils. This has the advantage, that a bake-out can be performed without removing the 3D-MOT optics, or one can simply measure the magnetic field.

Considering all of the above, a setup was implemented utilising two separate 2D-MOT chambers, to slow down the atoms, before loading then into a dual-species 3D-MOT. Using a 2D-MOT instead of a Zeeman slower has the advantage of a more compact setup and can therefore be more easily assembled on a translation stage. Aiming for the vacuum system to be on a translation stage also creates the constraint that the science chamber has to be connected by only one side. Usually, science chambers are glass cells since they ensure the best optical access. Unfortunately, the separated ovens for the species require angled atom inlets, which can not be manufactured as metal glass transition. That is were a compromise was made, in deciding for a rectangular metal science chamber. In order to ensure good optical access, manually sealed, elongated viewports are used instead of standard CF viewports. An overview of the setup is shown in figure 3.2.
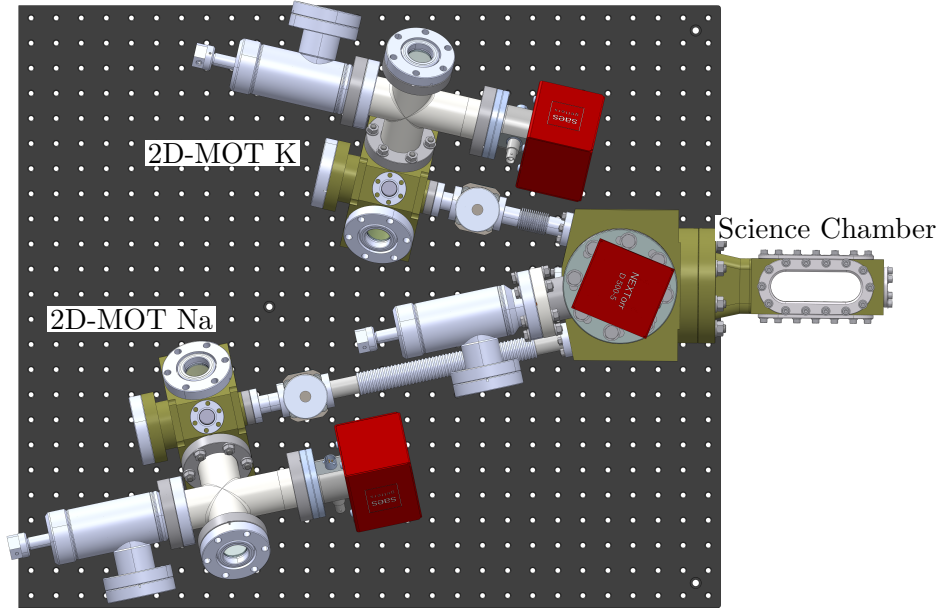
Figure 3.2: Setup of our vacuum system on the translation stage. Two identical 2D-MOT chambers are connected through bellows with the science chamber, one for each specie. To maximise the flexibility of the setup each chamber has an ion pump and a gate valve, which can be used to isolate them from each other.

The typical pressure ranges of a 2D-MOT and 3D-MOT do not overlap (see fig.3.1). To connect the 2D-MOT with the 3D-MOT, a differential pumping stage is used. This is nothing else than a tube limiting the gas flow between two chambers. For UHV and HV pressures the flow can be described by molecular flow, since the mean free path is long enough (fig. 3.1). The conduction C_{mol} is given by the length l and diameter d of the tube:

$$C_{mol} = 12.1 \frac{d^3}{l}. \tag{3.1}$$

The ratio of the conductance C_{mol} to the pumping speed S in the chamber with lower pressure equals the ratio of the pressures P in the two chambers:

$$\frac{C_{mol}}{S} = \frac{P_{Science}}{P_{2D-MOT}}. \tag{3.2}$$

Aiming for a pressure of at least 10^{-12} mbar in the 3D-MOT chamber ($S = 500\,\mathrm{l/s}$) and about 10^{-8} mbar in the 2D-MOT chamber, the diameter and length are chosen to be $d = 3\,\mathrm{mm}$ and $l = 30\,\mathrm{mm}$. [28]

3.1.1   *Chamber Geometry*

As already mentioned in section 3.1, the chamber design had to ensure good optical access, to use a non-magnetic material, and to have a

UHV sealing. In this section, a detailed overview of the geometry of the vacuum chambers, and the materials used, will be given. The 2D-
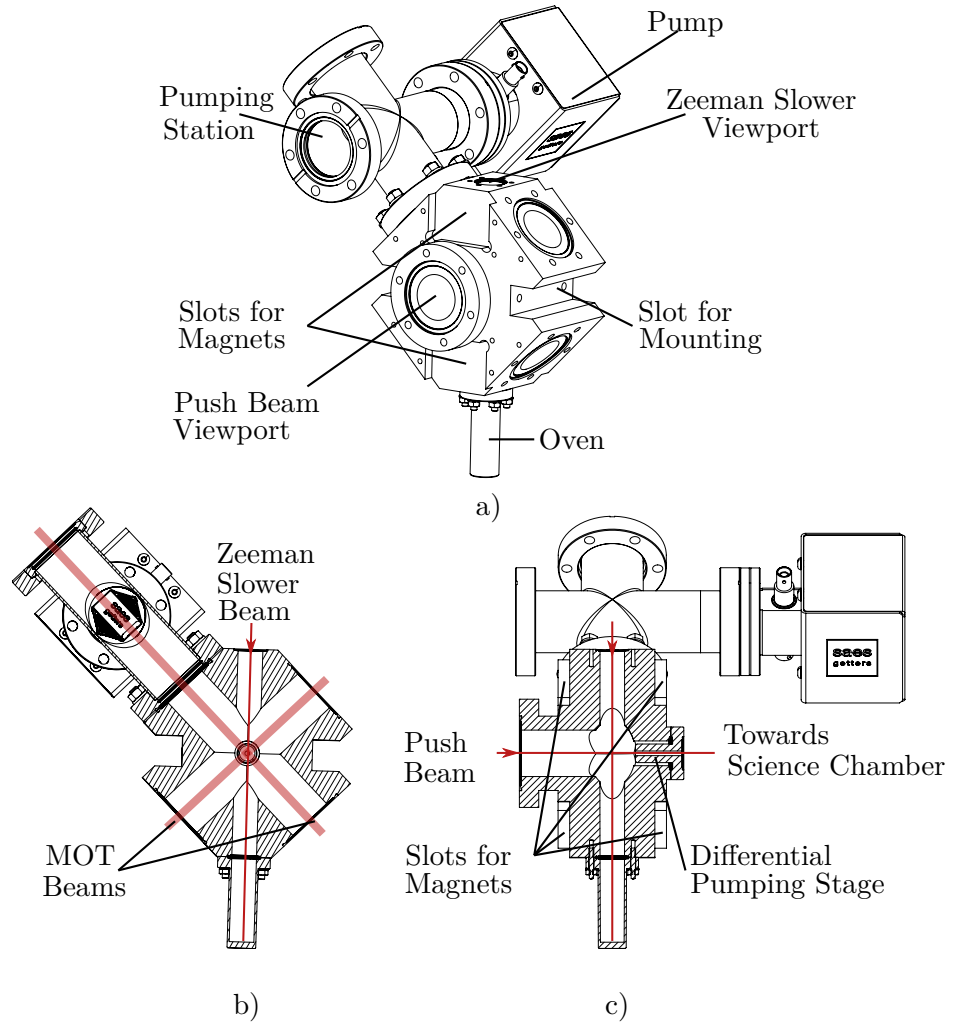
Figure 3.3: Drawings of the 2D-MOT chamber. (a) The compact chamber provides optical access via CF40 viewports for MOT beams. Two additional viewports are implemented, providing access for a Zeeman Slower beam and a push beam together with the imaging setup. The symmetrical chamber is extended on one side by a 4-way cross in order to attach an ion pump and pumping station. (b) Cross section of the plane spanned by the MOT beams. (c) Cross section spanned by the push beam and Zeeman Slower beam.

MOT chamber design (fig. 3.3) is inspired by Lamporesi et. al. [29]. The perpendicular 2D-MOT beams intersect in the centre of the chamber (made of titanium) in front of the differential pumping stage (fig. 3.3 b). At the top and the bottom of the chamber, there are CF16 connections for an oven (made of 316 stainless steel) and a viewport for the Zeeman slower beam (fig. 3.3 a,b). One 2D-MOT beam path is extended by a 4-way cross (made of 316 stainless steel) in order to mount the ion pump and to connect the pumping station (fig. 3.3 a). The front is equipped

with a CF40 viewport for the push beam, leaving enough space for imaging (fig. 3.3 a,c). The back is equipped with a CF16 flange connects the chamber with the bellows (made of 304 stainless steel) (fig. 3.3 c). There are slots on top and below the CF40 viewport and the Cf16 flange to place magnets (fig. 3.3 a,c). The left and right sides have slots for mounting the chamber(fig. 3.3 a,b).

Figure 3.4 shows two drawings of the science chamber design. The science chamber (made of titanium) has five viewports. Four of them are elongated. The dimension of the viewport at the top and the bottom is 90 mm×30 mm. The viewports on the sides are more narrow with 90 mm×15 mm. The science chamber is mounted to the so-called main chamber (made of titanium), where the atom beams of the two 2D-MOT systems are combined under an angle of 12.5°. The two atomic beams intersect in the centre of the science chamber.
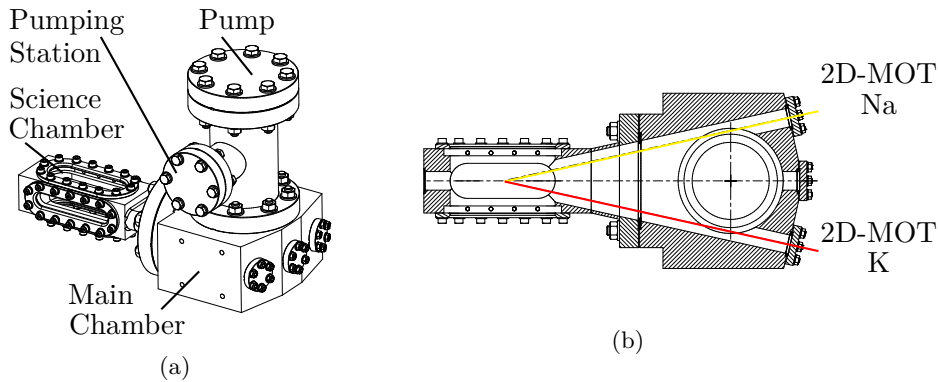
Figure 3.4: Drawings of the science and main chamber. (a) The science chamber is mounted to the main chamber, which connects the two 2D-MOT chambers. A tee-connector is used to mount the ion pump and the pre-pumping station. (b) Cutting through the plane spanned by the push beams. The sodium (yellow) and the potassium (red) atomic beams are intersecting at a 12.5° angle inside of the science chamber. An additional CF16 viewport is added to the main chamber and an opposing one to science chamber for aligning and monitoring purposes.

3.1.2 *Translation Stage*

The vacuum system is assembled on a translation stage, offering the following advantages:

- Instead of removing the 3D-MOT optics when performing a bakeout, the vacuum system can be easily moved away from the fragile optics.

- The possibility to measure the magnetic field gradient by simply moving the vacuum system away.

- The alignment of the beams can also be checked. However, the beams will have a lateral shift due to the refraction caused by the glass windows.

The idea for the translation stage was adopted from the group of Manuel Endres, California Institute of Technology [30]. They are using a translation stage from Lintech. However, these are either motorised or equipped with a hand-driven micrometer screw. The carrier dimensions are limited to either 152.4 mm or 304.8 mm. Taking the dimensions of the vacuum system, which is mounted on 600 mm ×700 mm breadboard, into account, it would be necessary to further stabilise the breadboard. The effective travel length will be reduced by the difference between sledge length and breadboard. For the translation stage the following requirements had to be met:

- `Effective Travel Length:` Possibility to pull the science chamber completely out of the coils.

- `Position:` Once positioned, the translation stage should not be able to move.

- `Repositioning:` When moving the system, it should get back to roughly the same position. The required precision of repositioning was estimated to a few millimetres, since this can be compensated by realigning the optics. Realignment is still a lot more convenient then rebuilding the optics.

- `Material:` Due to the magnetic sensitivity of the atoms, the translation stage should be non-magnetic.

- `Clean Operation:` The translation stage has to be mounted on an optical table. Therefore, the operation should be clean, i. e. possible dirt can come from lubricant or abrasion.

- `Easy and Quick Handling:` It should be easy and relatively fast to move.

- `Load:` The translation stage should be able to carry the whole system. We estimated the weight of our system to equal approximately 100 kg.

- `Assembly:` Building up the translation stage should be simple and fast.

With an approximated weight of 100 kg the vacuum system is light enough so that many different slide and rail systems are available.

Due to the breadboard size and the required length of the system, we were looking for a custom translation stage made out of building kit components. There are two bearing types to be considered: Rolling bearings and friction bearings. Rolling bearings have less friction, however, they need a lubricant, in most cases oil, which will cover the rails.

It is inevitable for the oil to spread over the optical table and thus attracting dirt. On the other hand, modern friction bearings, manufactured from high-performance polymer, can operate without a lubricant.

Considering this, the lubricant free friction bearings from Igus were chosen. It was decided to use the T25 rail system, since it is easy to assemble. The T20 series would have been sufficient to carry the load of the system, however, the rails have a M5 hole pattern requiring adapter plates to be mounted to the optical table. Therefore the T25 series with M6 hole patterns was used. The chosen system operated without a micrometer screw, which not only needs a lot of maintenance, but also would be rather bothersome to move the vacuum 42 cm.

The translation stage has a total travel length of 42 cm. The vacuum system is mounted in a way that the science chamber stands out and is thus easily accessible. Four guide carriages are mounted underneath the breadboard with a built-in clamping function, for short term positioning, as the holding forces will vanish over time. The final position is marked with angle brackets mounted to the optical table. For long term positioning, the breadboard is clamped in between two angle brackets.

3.2   EXPERIMENTAL TECHNIQUES

3.2.1   *Sealing with Indium*

The compact and modular vacuum system is mounted on a translation stage. Compromising in gaining flexibility with the translation stage, however, loosing the possibility of an all glass science chamber. The science chamber is manufactured out of titanium with elongated viewports, which had to be sealed with indium. Andrea Bertoldi, Institut d'Optique provided helpful advise on how to do indium seals. The indium seal, as shown in figure 3.5, consists of multiple layers of different materials.

To do an indium sealing, the following steps have to be followed:

1. `Shaping:` The indium wire has to be shaped into the desired form. This step was practised with a 3d printed model of the science chamber and soldering wire. It was also helpful to estimate the required wire length. Shaping the indium wire is more difficult than the soldering wire, as the wire bents easily under its own weight and is very sticky.

2. `Placing:` After the wire was shaped, it was carefully placed in the retaining edge of the science chamber, trying to correct the shape, so that the wire is nicely centred everywhere (figure 3.6 a). Furthermore, it was ensured that the two ends of the wire overlap. After the wire is placed, the glass can be carefully placed on top of it.
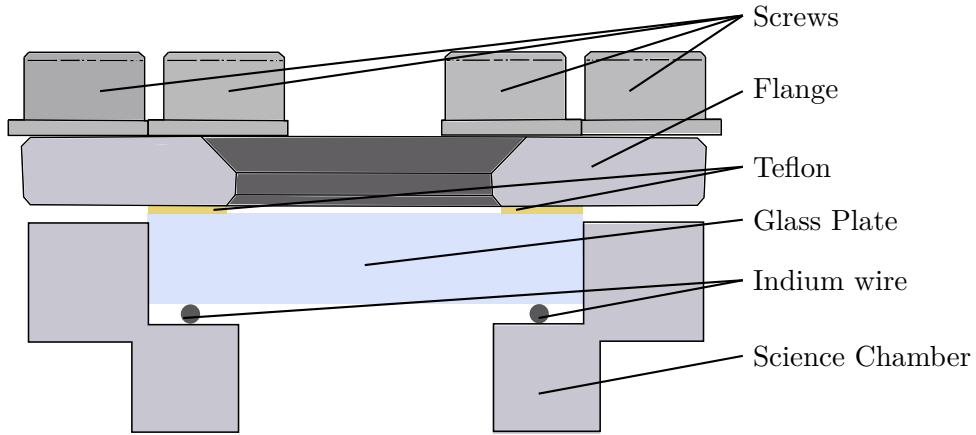
Figure 3.5: The layers of different materials for an indium sealing. The indium wire, which will get compressed, is placed between the chamber and glass plate. To protect the glass plate, a sheet of Teflon is put between the glass and the flange.

3. `Flange Preparation:` To protect the glass, a layer of 0.1 mm Teflon tape is placed on the flange. The Teflon is fixed with Kapton tape (figure 3.6 b).

4. `Screwing:` The prepared flange is carefully placed on the glass (see fig. 3.5 and 3.6) and all screws are slightly fastened. Finally the screws are tightened in small steps.
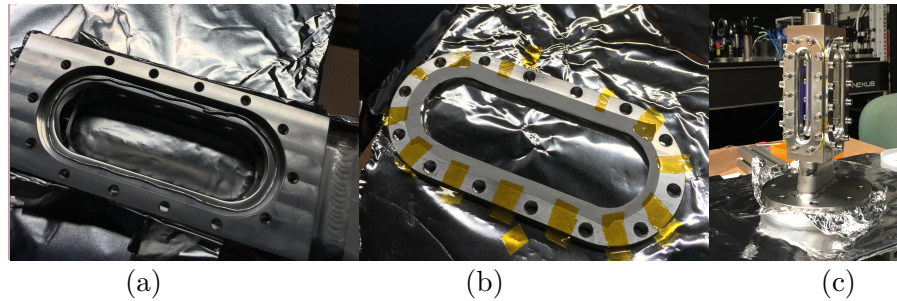
Figure 3.6: The process of sealing our science chamber. (a) The indium wire is shaped and placed, so that it is centred on the retaining edge. (b) The flange is prepared with a layer of Teflon, which is held in place with Kapton tape. (c) The completely sealed science chamber.

3.2.2 *Pumping*

A series of different pumps is needed to get from one vacuum region to another. When pumping down the vacuum, these pumps are turned on in succession, making sure that the pressure is within the operating range of the current pump (see. fig. 3.1).

Oil-Free Scrolling Pump: An oil free scrolling pump, is used to pump down from atmospheric pressure to a medium vacuum. It consists of two spirals, one is orbiting against the other, such that gas gets trapped and compressed towards the centre, where it is pumped out. In figure 3.7 the compression of gas is illustrated. Because the two spirals do not grind against each other, the operation is oil-free. [31]

Figure 3.7: The scrolling pump compresses the gas using two spirals (black and orange) moving against each other. Gas gets compressed while travelling to the centre where it is exhausted. The compression is indicated by a darker colour. Since this process takes 3.5 cycles of the spirals, new gas is trapped and compressed simultaneously. Figure adopted from [31].

Turbo Molecular Pump: A Turbo Molecular Pump (TMP) pumps a medium vacuum down to a UHV vacuum. The basic concept of a TMP is to manipulate the trajectory of particles by a moving wall (Holweck pump). This only works, if the mean-free path of the molecules is sufficiently large, so that only collisions with the walls are important, i. e. , collisions between particles are negligible. The TMP is an improved version of the Holweck Pump, which uses the tennis principle where a molecular flow is built-up by transferring an momentum to the molecules using rotors (fig. 3.8). This is only possible, if the velocity of the rotor blades is close to the thermal velocity of the molecules. [26, 32]

Ion Pump: The Ion pump consists of two parts: A non-evaporable getter element (NEG) and an ion element. The majority of gases are pumped by the getter material, whereas the ion element pumps the gases that are not affected by the getter material, e. g. methane or argon. The ion element uses magnetic and strong electric fields to ionise molecules and atoms, which are accelerated towards the grounded cathode and are bound chemically. These processes are illustrated in figure 3.9. The NEG element has to be reactivated (heated) if saturated. During the reactivation process hydrogen recombines on the surface, whereas reacted components e. g. carbon-dioxide diffuse into the bulk material of the NEG element.[26]
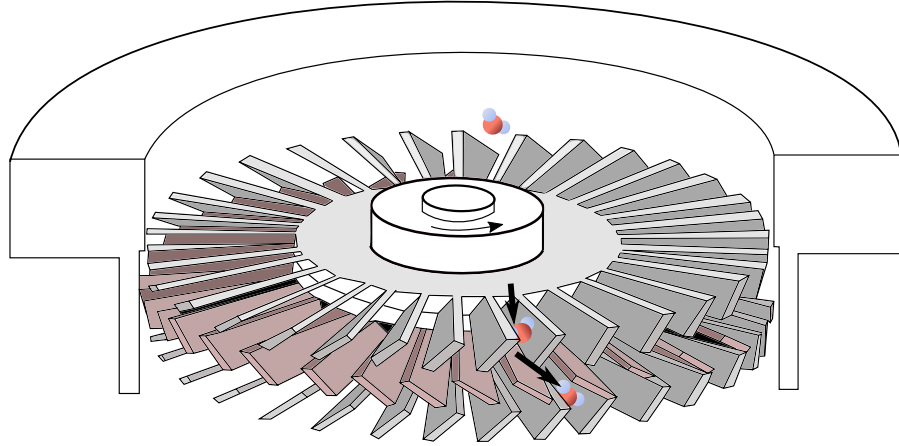
Figure 3.8: The Turbo Molecular Pump consists of several layers of rotors, alternating between rotatable ones (grey) and static ones (red). The rotors move with a velocity close to the thermal velocity of the molecules, so that a molecule, that gets between the rotor blades, receives an impulse to the bottom. The static rotor blades decelerate the molecules and compress the gas. Figure adopted from [32].
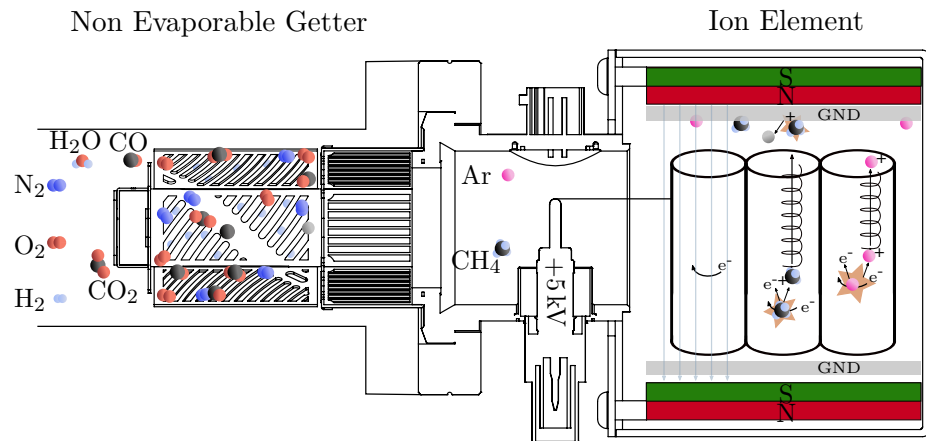
Figure 3.9: The Ion pump consists of two parts: A non evaporable getter (NEG, left) and an ion element (right). Active gases that hit the getter surface dissociate into their components and/or react with the getter material on the surface. Dissociated Hydrogen diffuses into the bulk material. Non-active gases and noble gases, e. g. methane or argon, are not affected by the getter material. The ion element consists of two magnets creating a homogeneous magnetic field and a high electric field (5kV). Free electrons are attracted to the positive anode. Due to the magnetic field, they are trapped in a circular movement. Molecules and atoms are ionised by collisions with those electrons, creating new electrons that are forced on a circular trajectory as well. The ions, on the other hand, are accelerated to the cathode, where they bound chemically to the material. The impact can spatter some atoms of the cathode material. [26] Figure adopted from *SEAS Getters* and *GammaVacuum* [33].

3.2.3 *Bake-out*

After pumping a vacuum system down, e. g. with a TMP, the spectra
recorded with a residual gas analyser (RGA) reveals that the pressure is
limited by water. In general, one would suspect the TMP to be limited
by hydrogen. However, water depositions are all over the walls and
slowly degrading from the walls over time, resulting in a limitation by
water. The degrading process can be accelerated by performing a bake-
out, where the whole system is being heated, using temperatures up to
300 °C.

   The system should be heated up homogeneously and is therefore
limited by the maximum operation temperatures of the components. To
monitor and control the heat up numerous thermocouples have to be
placed on the setup. Since stainless steal has a low thermal conductivity,
the system is covered in a laxer of aluminium-foil in order to spread
the heat equally. Glass-fibre heating tapes are wrapped around equally,
before everything is covered again with a layer of aluminium-foil. A
slow increase of temperature (e. g. $\frac{1\,°C}{\min}$) has to be ensured for a bake-
out containing glass components, to avoid damage by thermal tensions.
It turned out that the pumping speed of the pump in the 2D-MOT
chamber is large enough to achieve an appropriate vacuum (10^{-10} mbar)
without performing a bake-out. For the science chamber a bake-out was
performed, that was limited to 110 °C, due to the indium seal.

3.2.4 *Procedure to Fill the Oven*

Once the atomic source is exhausted, it is necessary to (re)fill the oven
with an atomic source. The oven was first filled, after it was ensured
that the vacuum system was in the desired pressure region. To stack
the oven we pursued the following steps:

1. `Preparation:` The outside of the ingot ampoule is cleaned with
    acetone. The glued label has to be removed. Tools that are re-
    quired to smash the ampoule have to be cleaned as well.

2. `Flooding System with Nitrogen:` There are two reasons why
    the chambers are flooded with nitrogen. First of all, alkali metals
    react with water and oxidise, secondly our ion pumps are sensitive
    to contact with air. The vacuum system was flooded with nitrogen
    using the glove technique, instead of a dosing valve. Therefore, the
    nitrogen bottle was connected with a powder free glove which is
    connected to the ventilation valve (vent valve) of our pumping
    stage. The glove is used as a balloon to indicate the pressure.
    The system is flooded by repeating the following two steps:

    a) Vent valve is closed. Carefully inflate the glove.

b) Nitrogen bottle is closed. Slowly open the vent valve to let nitrogen into the system. However, one must be cautious for the glove not to be sucked into the vent valve.

These steps are repeated until the glove does not deflate any more when opening the vent valve. While opening the oven and filling it, a flow of nitrogen through the chamber is created. When opening the vent valve and the gas bottle, constantly check for the glove to not inflate.

3. `Filling the Oven:` Unmount the oven and place the ampoule inside. Then smash the ampoule e. g. using a screw driver and hammer. Quickly mount the oven back to the chamber.

3.3 CONCLUSION

In this section the practical advantages and disadvantages of the setup are discussed.

A compact and modular design was implemented. The modularity of the setup provides the possibility to work independently on the pre-cooling steps of the two species and to operate with only one specie, e. g. maintain the setup of one specie while keep the other running. Building both species up out of the same modules, provides the advantage that the gained knowledge can be used for the other specie. The translation stage has already been very useful for alignment and magnetic field measurements. Stability issues might be a drawback of the translation stage, however none occurred so far. Due to the translation stage, one had to compromise at the science chamber, which limits the bake-out temperature to $110\,°C$ due to the indium seal and has lesser optical access then a glass chamber. So far, the optical access is sufficient and the lower bake-out temperatures did not lead to any significant disadvantages. In the 2D-MOT chambers, we were even able to achieve a UHV vacuum without performing a bake-out, due to the high pumping speeds of the pumps.

The 2D-MOT chambers are connected by bellows to the main chamber, which were intended to enhance the flexibility. However, they also add a degree of freedom, which makes it very hard to level the whole setup. On the other hand, it would have been a lot more difficult to connect the chambers without bellows.

In general, a compact vacuum system is favourable. Nevertheless, this also leads to difficulties e. g. when accessing the oven. The oven is welded to a CF16 flange and designed to have a maximal possible inner diameter. Therefore, it is not possible to screw the oven with nuts instead of a wrench.

Assembling the 2D-MOT optics and heaters, we came up with the following improvement. It might be better to add a nipple or a CF16 to CF40 adapter between chamber and oven, resulting in lesser distur-

bances of the magnetic field and a larger and easier accessible oven. Adding a nipple between chamber and upper viewport would result in more space to mount optics and heaters. When setting up the 3D-MOT, we noticed that it might have been wise to add an opening in the breadboard underneath the main chamber, freeing up some space for optical posts. This will be further discussed in chapter 6.

3.4 SUMMARY

For an ultracold atom experiment a good UHV is needed, since atoms would heat up due to collisions. A UHV vacuum can not be achieved with a single pump. In our setup we use a pumping stage consisting of a scrolling pump, a turbo molecular pump and a residual gas analyser to get a preliminary vacuum and test our setup for leaks. As a permanent pump we use an ion pump. The required pressure for a 2D-MOT (10^{-8} mbar) is different from the pressure required for a 3D-MOT. In order to connect these pressure regions with each other a differential pumping stage was added.

The experimental techniques on how we performed an indium seal and how we flooded our system was described.

Our aim was to build a compact and modular vacuum system. To do so we had to compromise on the optical access, the possible bake-out temperature of our science chamber, and the accessibility of our oven.

For the translation stage, which gives us the advantages of being able to move the vacuum system out of the magnetic field coils without disturbing the 3D-MOT optics, a simple, clean, and low cost version was found.

LASER TABLE

So far it was discussed how to set up a vacuum, in order to create the appropriate environment for the atoms. The motions of the atoms can be manipulated with light as it is reviewed in section 2.1. However, for these techniques, light at a certain frequency is needed. A laser itself is not sufficient for this task: Although lasers do operate very stable the frequency will drift, e. g. due to temperature fluctuations. Additionally, beams with light at frequencies differing in the MHz to GHz range are needed, e. g. for repumping and cooling. The best way to set the frequency of a laser and stabilise it, is to use the atoms themselves as reference in a spectroscopy scheme. The frequency stabilised light is then split up in several paths, where the beams are shifted in frequency. All these steps are combined on a laser table.

The following light paths are needed for the setup: A spectroscopy path, a path for the 2D-MOT, one for the 3D-MOT, a push beam to push the atoms from the 2D-MOT into the 3D-MOT region, as well as a slower beam to slow down the atoms, which evaporate out of the oven. Since wavelengths of atomic transitions of sodium (589 nm) and potassium (767 nm) differ a lot, all paths are needed for each species. To keep the setup modular, the laser tables have been separated. The aim is to work with ^{40}K and ^{39}K, therefore, the potassium laser table has to be designed in a way that it is possible to switch from one isotope to the other.

In this section, the different aspects of the two laser tables are discussed starting with the generation of light.

4.1 LIGHT GENERATION

Diode lasers are cost effective and very efficient. The wide gain profile leads to the creation of many modes. To achieve single mode operation a grating is used, e. g. in Littrow-configuration is used. A selected mode is reflected back to the diode, which forces the laser into single-frequency operation. The frequency can be tuned by the choice of a different mode. This is done by the change of the angle of the grating. For a high beam quality, a small aperture is needed, limiting the output power of the diode laser to several tens of mW, since too high powers could damage the diode. In order to achieve laser powers of a few Watts an additional amplification stage is used. Nowadays, a wide range of wavelengths of diode lasers is available, where non linear frequency conversion techniques did close the gaps in wavelength regimes. [34]

The required wavelength of 767 nm for potassium can be generated by standard diode lasers. For this setup, a commercially available *DL pro* laser from *Toptica* was used. This laser gets amplified by a home-built tapered amplifier (TA) (design from [35]). A TA is a semiconductor optical amplifier that consists of two sections: A lateral single mode section and a tapered region. The light gets amplified in the tapered region, while the output density is reduced, by diverging the beam. Therefore, the beam has to be reshaped afterwards. [34] More details about the TA are given in [36].

The required wavelength of 589 nm for sodium can not be achieved with standard laser diodes. The commercially available *TA SHG Pro* laser from *Toptica* comprises three components: A 1178 nm diode laser, a TA and a second harmonic generation (SHG) cavity. In the SHG cavity, two photons are converted inside a non linear crystal into a photon of half the wavelength. [34]

To ensure that the frequency of the laser is set correctly, a small amount of the light is used for a reference spectroscopy.

4.2   FREQUENCY SETTING

If a laser is sent through an atomic vapour cell and detected afterwards, the absorption will be observed as a reduction in intensity at the atomic resonance frequency of the laser. However, due to the Doppler effect, the thermal velocity distribution of the atoms will lead to a spectral broadening. In order to resolve the hyperfine splitting, a Doppler free absorption spectroscopy scheme (fig. 4.1b) is needed. Here, the laser is reflected, so that only atoms with velocity $v = 0$ are resonant with both laser beams. For multilevel atoms, additional peaks and dips, the so-called crossover resonances, can be observed. These result from atoms with velocities $-v$ and $+v$ and are therefore resonant to two different atomic transitions(ω_1 and ω_2). Depending on whether the transitions have the same ground or excited state, increased or decreased absorption can be observed at $\frac{\omega_1+\omega_2}{2}$.

In table 4.1 some of the atomic properties are summarised. Both species

Table 4.1: Atomic properties of sodium and potassium. Data taken from [37] and [38].

	Abundance [%]	Lifetime	Nuclear Spin	Vapour Pressure [mbar]	
^{23}Na	100	stable	3/2	$2.9 \cdot 10^{-11}$, 25 °C	bosonic
^{39}K	93.25	stable	3/2	$1.3 \cdot 10^{-8}$, 20 °C	bosonic
^{40}K	0.01	$1.28 \cdot 10^9$ y	4	$1.3 \cdot 10^{-8}$, 20 °C	fermionic
^{41}K	6.73	stable	3/2	$1.3 \cdot 10^{-8}$, 20 °C	bosonic

have a low vapour pressure at room temperature, hence it is necessary
to heat the spectroscopy cell to observe a spectroscopy signal. We used
two mineral insulated band heaters, which are mounted onto brass cylin-
ders with a small hole for the laser beam to pass through (fig. 4.1a).
The gap between the brass cylinders functions as cold spot, ensuring
that the laser path is not getting blocked by Na/K deposits on either
side of the vapour cell.

(a) Vapour Cell Assembly

(b) Doppler Free Saturated Absorption Spec-
troscopy Setup
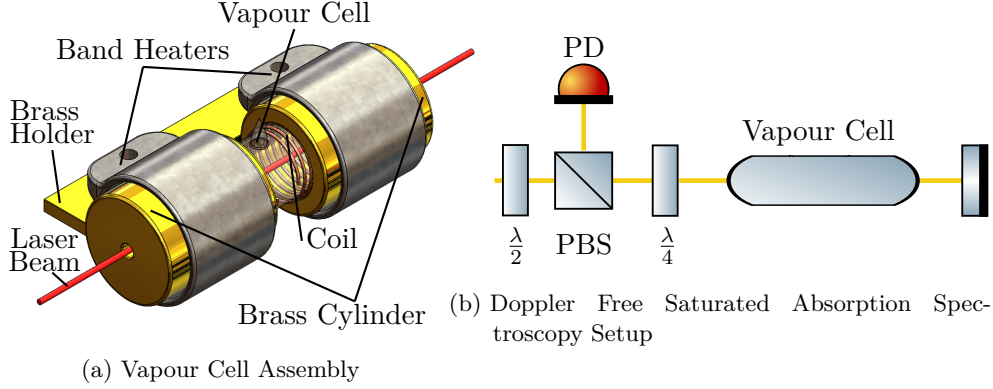
Figure 4.1: (a) Assembly of the vapour cell, including band heaters and a coil
for magnetic field modulation (taken from [36]). (b) Doppler free
saturated absorption spectroscopy setup.

The spectroscopy cell is heated to approximately $130\,°C$ for sodium and
$60\,°C$ for potassium. The temperature is controlled by a control circuit,
which is further described in section 5.1. For potassium and sodium, the
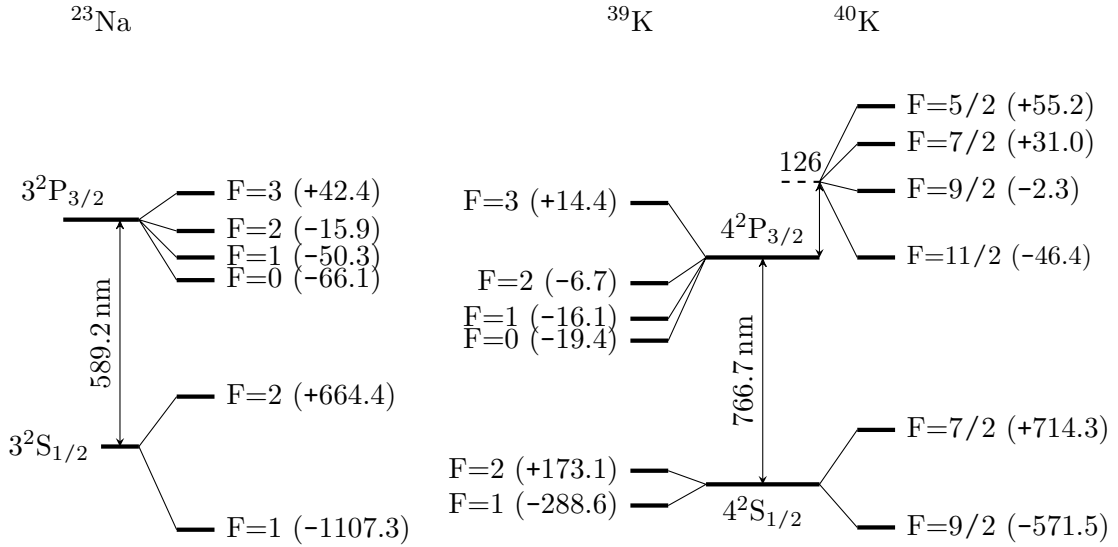
Figure 4.2: D2 lines of ^{23}Na, ^{39}K and ^{40}K. Level energies are given in MHz.
(Figure not to scale)

ground state splitting of the D2 line is quite large, whereas the upper
states are only separated by a few MHz (see fig. 4.2). Therefore, it is not
possible to resolve the upper states. ^{39}K is the potassium isotope with

the highest natural abundance of 93% (see table 4.1). Consequently, the contribution from the other isotope is negligible. In figure 4.3, the spectroscopy signals of the D2 line of sodium and potassium are shown. For both species, the two ground state peaks and the corresponding crossover dip (central dip at 0 MHz detuning) can be identified. With

(a) Spectroscopy Signal of ^{23}Na   (b) Spectroscopy Signal of ^{39}K
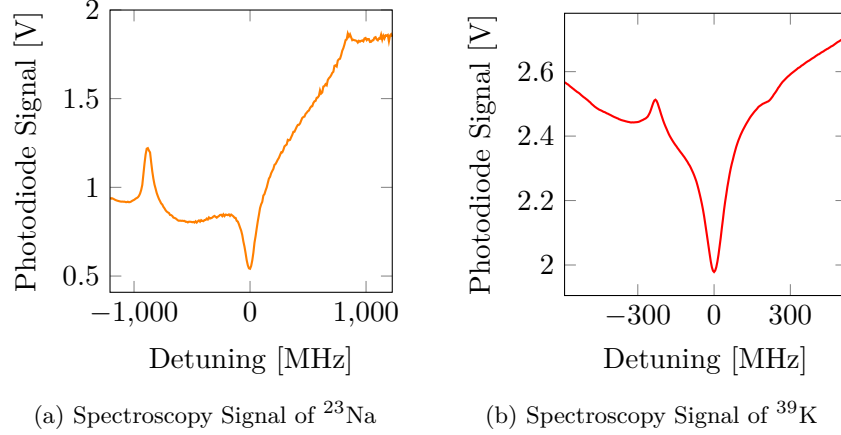
Figure 4.3: The spectroscopy signals of sodium (a) and potassium (b). For both species the separation of the $^2P_{3/2}$ state is only a few MHz so that only the hyperfine structure of the $^2S_{1/2}$ can be resolved: Peak on the left $F_g = 2$, peak on the right $F_g = 1$ and central dip is the crossover resonance of the two ground states.

these spectroscopy signals it might be possible to tune the laser on one of these transitions. Unfortunately, the laser is very sensitive to disturbances, e. g. temperature fluctuations or pressure variations in the lab, and will therefore drift in frequency.

4.3   FREQUENCY STABILISATION

To stabilise the frequency of the laser to an atomic transition, a feedback loop is needed (fig. 4.4). For this purpose the spectroscopy signal is not appropriate. A small disturbance in frequency results in small changes of the amplitude only. Furthermore, no informations about the sign of the frequency change can be obtained. Therefore, a dispersive signal, the so-called error signal, is created by modulating the frequency. The offset of the dispersive signal can be set, such that the position of the peak corresponds to the zero crossing. Small disturbances in frequency will result in a large change in amplitude, due to the slope, and the sign tells in which direction the frequency has to be corrected. For the feedback loop, a small amount of the laser light is taken to generate the spectroscopy signal, which is modulated by a sinusoidal signal from a function generator. The reference signal, that can be a rectangular signal of the same frequency, and the modulated spectroscopy signal, are fed into the Lock-In amplifier, which generates the error signal, a
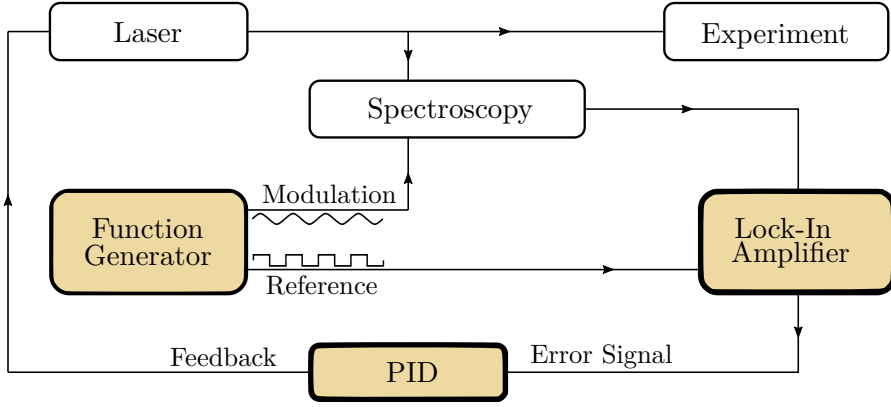
Figure 4.4: Schematic of a feedback loop, used to stabilise the frequency of a diode laser. The coloured devices can be combined in a *STEMlab Red Pitaya* board.

signal proportional to the derivate. The PID compares the signal with the setpoint and gives the feedback parameters to the laser driver.

The Lock-In amplifier generates the dispersive signal by mixing the spectroscopy signal with the reference signal [39]. Compared to the modulation frequency [kHz], the frequency scan of the laser [Hz] is very slow. Therefore, the intensity I can be Taylor expanded around the frequency ω_0

$$I(\omega) = I(\omega_0) + \frac{\mathrm{d}I}{\mathrm{d}\omega}_{|\omega=\omega_0} (\omega_0 - \omega) + ... \tag{4.1}$$

with the frequency modulation $\omega(t) = \omega_0 + \Omega_0 \cos(\Omega t)$ we get

$$I(\omega) = I(\omega_0) + \frac{\mathrm{d}I}{\mathrm{d}\omega}_{|\omega=\omega_0} \Omega_0 \cos(\Omega t) + ... \tag{4.2}$$

Mixing the spectroscopy signal I with the reference signal $U_{\mathrm{ref}} = \cos \Omega t + \phi$, shifted by a phase ϕ, gives

$$U_{\mathrm{ref}} \cdot I = I(\omega_0) \cos(\Omega t + \phi) \tag{4.3}$$

$$+ 1/2 \Omega_0 \frac{\mathrm{d}I}{\mathrm{d}\omega}_{|\omega=\omega_0} \cos(2\Omega t + \phi) \tag{4.4}$$

$$+ 1/2 \Omega_0 \frac{\mathrm{d}I}{\mathrm{d}\omega}_{|\omega=\omega_0} \cos(\phi). \tag{4.5}$$

Applying a low-pass filter, cuts off all high frequency terms, resulting in the output signal

$$U_{\mathrm{ref}} \cdot I = 1/2 \Omega_0 \frac{\mathrm{d}I}{\mathrm{d}\omega} \cos(\phi), \tag{4.6}$$

which is proportional to the derivative of the transmitted frequency. Most commonly, the frequency is modulated by directly modulating the laser current. This is easy to implement, however, it has the disadvantage that the modulation effects the whole laser table. Thus, the

magnetic field is modulated in this setup. Due to the magnetic field, the level splitting of the atoms is modulated, effectively changing the frequency of the laser for the atoms. Therefore, a coil (150 windings of 1mm copper wire) is wound around the spectroscopy cell, before the brass cylinders with the band heaters are placed (see fig. 4.1).

Aiming for a compact design, the number of devices to lock the laser, is reduced by using the *STEMlab* board *RedPitaya*. It combines Lock-In amplifier (iq module), function generator, PID controller and digital oscilloscope when using the open source graphical user interface *PyRPL* (indicated in figure 4.4). The board can not provide enough current to modulate the coils. Therefore, a commercial current amplifier (*OPA548*) board is used. The resulting error signals are shown in figure 4.5. With a modulation frequency of 10 kHz, the laser is currently locked to an atomic transition for several hours.

(a) Error Signal of ^{23}Na

(b) Error Signal of ^{39}K
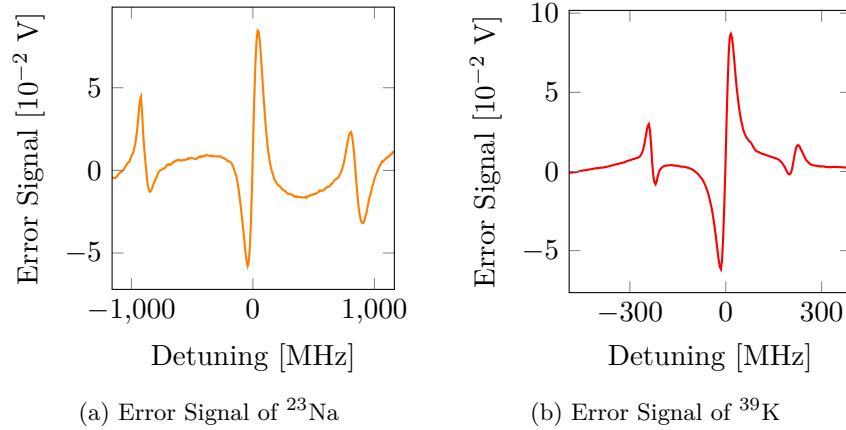
Figure 4.5: Error signals of sodium a) and potassium b). For both species the separation of the $^2P_{3/2}$ state is only a few MHz so that only the hyperfine structure of the $^2S_{1/2}$ can be resolved. The central feature is the crossover resonance of the two ground states, on which the error signals are optimised.

4.4   FREQUENCY MODIFICATION

So far, the laser frequency is stabilised to an atomic transition. However, light with different detuning, with respect to various transitions, is needed for the applications. Since the exact detuning, values are obtained experimentally e.g. by optimising the 3D-MOT loading rate, the detuning should be easy to change. The light is coupled into single-mode fibres, which are very sensitive regarding beam alignment. Frequencies can be efficiently shifted by acousto-optical modulators (AOMs) and electro-optical modulators (EOMs). In both cases, the frequency is shifted by applying an RF-voltage, generating higher orders in frequency (figure 4.6). Concerning AOMs, a sound wave, travelling through

(a) Acousto-optical modulator

(b) Electro-optical modulator
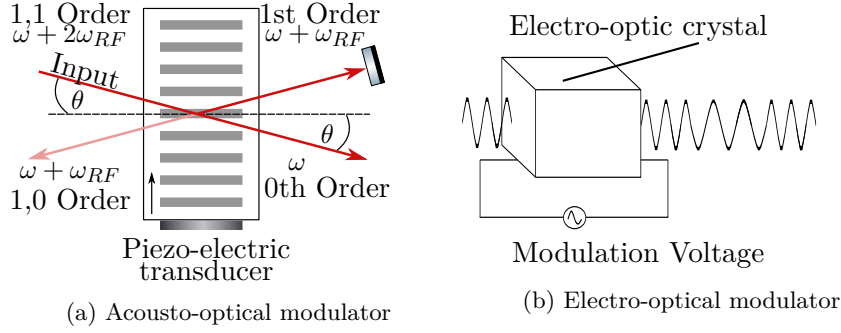
Figure 4.6: Two ways of efficient frequency modulation of light. (a) An AOM consits of a crystal, which refractive index is modified through density variations. These are caused by sound waves generated by a piezo-electric transducer, driven with frequency ω_{RF}. A incident beam under an angle θ will be split up into multiple orders denoted by n, that are spatially separated by an angle $\pm 2n\theta$ (on the right). The frequency is changed by $\pm n\omega_{RF}$. In double-pass configuration, the first order is reflected by a mirror and is split up again. The first order of the back-reflection (1,1 order) is exactly superimposed with the incoming beam.[40, 41] (b) An EOM consists of an electro-optical crystal, whose refractive index can be changed by applying a RF-voltage (Pockels effect). The phase shift of the output beam translates to a frequency modulation.[41, 42]

the crystal, causes a variation of the refractive index. This acts as a diffracting grating, where incident light is spatially separated into multiple diffraction orders. In EOMs, the refractive index is modulated due to the Pockels-effect. This modulation creates frequency side-bands.

Operating AOMs in double-pass configuration has the advantage that the beam path is independent for the same in and out coming orders. A convex lens mirror pair (cat's eye retro-reflector) is used to increase the range of RF-frequencies, in which high efficiencies can be achieved. Therefore, the detuning can be tuned without disturbing the beam path. [40, 41]

4.4.1 *Sodium*

Figure 4.7 illustrates the laser table layout of sodium. The $F_g = 2$ to $F_e = 3$ transition is used for cooling and the $F_g = 1$ to $F_e = 2$ transition is used for the repumper. Before being locked to the $F_g = 2$ transition peak, the frequency is shifted by an AOM double pass (1,1 order). The light that is supplied to the other beam paths, is therefore red-detuned with respect to the locking transition. The cooling light is generated by an AOM double-pass, extracting only the (1,1) order. Additionally, the repumping light is produced by the first order of an EOM. For the slower, the -1st order of an AOM single-pass is used to create the cooling frequency followed by an EOM to generate the repumper light. The push beam does not require a repumper and is therefore, generated
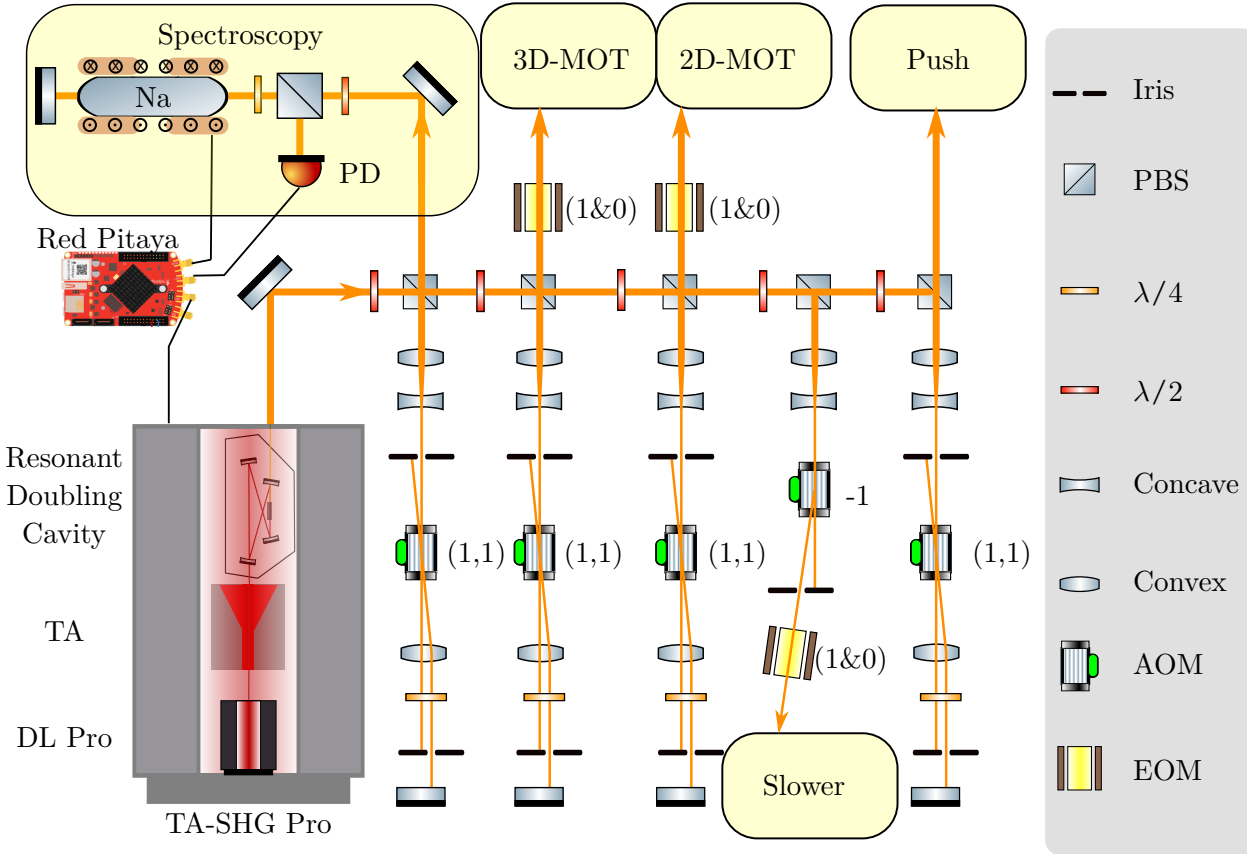
Figure 4.7: Schematic of the sodium laser system. The laser consist of a *DL pro*, a tapered amplifier, and a resonant doubling cavity for yellow (589 nm) light generation. The light is divided into five paths: Spectroscopy, 3D-MOT, 2D-MOT, Push beam, and Slower. For each path, the frequency is shifted by AOMs for the cooling transition and EOMs are used to generate the repumping light. The spectroscopy delivers the signal for the frequency stabilisation. The *Red Pitaya* replaces the Lock-in amplifier, PID controller, and signal generator. Figure adopted from [36].

by only one AOM-double pass taking the (1,1) order. Starting values for power distributions and detunings were obtained from Gretchen Campbell's group at the Joint Quantum Institute (JQI). The planned values are summarised in table 4.2.

4.4.2 *Potassium*

For potassium, the laser table is more complicated, since we would like to be able to switch between the two isotopes ^{39}K and ^{40}K. A beat lock is installed to switch from one istope to the other (fig. 4.8): A master laser is stabilised to an atomic transition, whereas the slave laser is locked to a tunable frequency offset with respect to the master laser. The beat signal is generated by superimposing the light of the master ω_M and the slave ω_S on a fast photodiode, with which only the

Table 4.2: Planned detuning and powers of the different light paths for Sodium. Saturation intensity is $6.26\,\mathrm{mW/cm^2}$.

	Transition $F_g \rightarrow F_e$	Detuning [MHz]	Power** [mW]	Beam diameter [mm]
Spectroscopy*	$F_g = 2 \rightarrow F_e$	-150	10	2
2D-MOT				
cooling	$2 \rightarrow 3$	-9	116	10
repump	$1 \rightarrow 2$	-12	92	10
3D-MOT				
cooling	$2 \rightarrow 3$	-9	250	10
repump	$1 \rightarrow 2$	-12	35	10
Slower				
cooling	$2 \rightarrow 3$	-299	73	10
repump	$1 \rightarrow 2$	-299	4	10
Push	$2 \rightarrow 3$	+6	5	2

*Values are given for the light before the double-pass.
**The given powers are used to calculate the total power needed.

difference $\Delta\omega = \omega_S - \omega_M$ can be detected. Mixing this signal with a radio-frequency signal and cutting higher frequencies off results in a signal with frequency $\Delta\omega - \omega_{\mathrm{RF}}$. The signal is split and a frequency-depending phase shift $\phi = (\Delta\omega - \omega_{\mathrm{RF}})\tau$ between the two signals, is generated by a delay line. The two signals are mixed together and the high frequency parts are removed by a low-pass filter, resulting in a signal proportional to $\cos(\phi)$, used as an error signal. The offset can be simply tuned by the RF-frequency, being limited by the chosen low-pass cut-off frequencies.

An overview of the potassium laser table is shown in figure 4.9. 3D-MOT, 2D-MOT and Slower beams are passing through two AOM double-passes. The first AOM generates the cooling light for both species taking the (1,1) or (-1,-1) order, whereas the second one is used to create the repumper for ^{39}K taking the (1,1) and (0,0) orders. The EOMs generate the repumper for ^{40}K. The push beam does not need a repumper, such that a single double-pass is used. With this setup, it is possible to switch between the two species by simply changing the offset of the beat lock and and turning off the second AOM and switching on the EOM, or the other way around. For ^{39}K (^{40}K) the $F_g = 2 \rightarrow F_e = 3$ ($7/3 \rightarrow 9/2$) transition is used for cooling, whereas the $F_g = 1 \rightarrow F_e = 2$ ($9/2 \rightarrow 11/2$) transition is utilised for the re-pumper beams. The planned detunings with respect to these transitions are summarised in table 4.3.
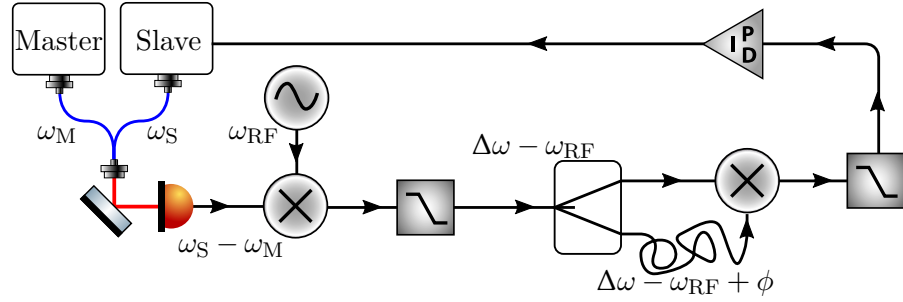
Figure 4.8: Schematic of the offset lock. The difference in frequencies of the superimposed light of Master and Slave is detected by a photodiode. The signal is mixed with an RF-signal and high frequencies are removed by a low-pass filter. The signal is split in two paths. In one path, the signal passes through a delay line acquiring a frequency-depending phase ϕ. The phase-shifted signal is then mixed with the original one before they pass through another low-pass filter. The resulting signal is used as an error signal to lock the slave laser. Figure taken from [36].

Table 4.3: Planned detunings for Potassium ^{39}K and ^{40}K.

	^{39}K		^{40}K	
	Transition	**Detuning**	**Transition**	**Detuning**
	$F_g \to F_e$	[MHz]	$F_g \to F_e$	[MHz]
Slave	crossover of ^{39}K	-410	crossover of ^{39}K	+406
2D-MOT				
cooling	$2 \to 3$	-16	$9/2 \to 11/2$	-10
repump	$1 \to 2$	-15	$7/2 \to 9/2$	-10
3D-MOT				
cooling	$2 \to 3$	-26	$9/2 \to 11/2$	-20
repump	$1 \to 2$	-15	$7/2 \to 9/2$	-20
Slower				
cooling	$2 \to 3$	-335	$9/2 \to 11/2$	-330
repump	$1 \to 2$	-335	$7/2 \to 9/2$	-330
Push	$2 \to 3$	-5	$9/2 \to 11/2$	0

3D-MOT
cooling,
repump

-1 & 0

1,1 & 0,0

1,1

2D-MOT
cooling,
repump

-1 & 0

1,1 & 0,0

1,1

Slower
cooling,
repump

-1 & 0

1,1 & 0,0

-1,-1

1,1

Push
beam

| | Mirror | | $\lambda/2$ | | Convex | | PBS | | AOM ^{39}K repump |
| | Iris | | $\lambda/4$ | | Concave | | EOM ^{40}K repump | | AOM ^{40}K, ^{39}K cooling |
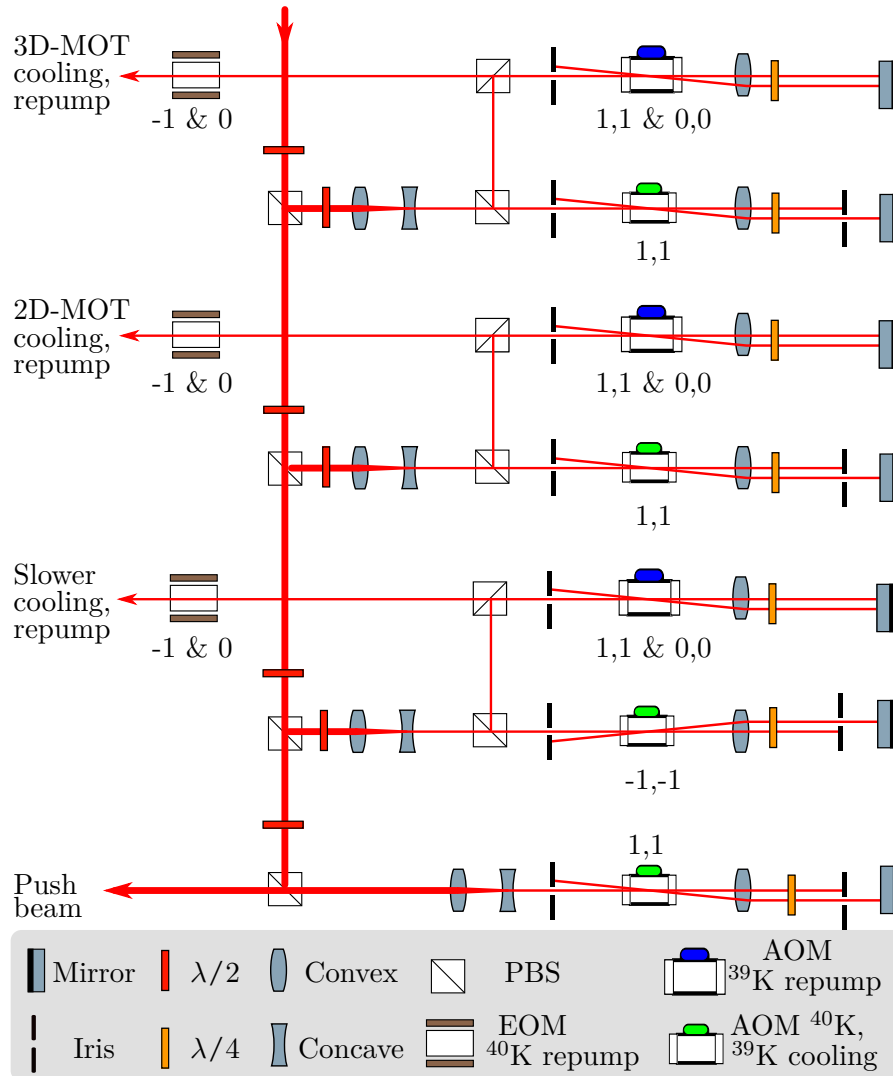
Figure 4.9: Schematic of the potassium laser table. Each beam is reduced in
diameter in order to fit through the AOM's aperture. 3D-MOT,
2D-MOT and Slower beams are passing through two AOM double-
passes. The green AOM shifts the frequencies required for cooling
for both isotopes. The second AOM (blue) produces the repumper
for ^{39}K, while the EOM creates the repumper for ^{40}K. For the
push beam only one double pass is used since no repumping light
is needed. Figure is taken from [36].

4.5 CONCLUSION

In this section, the light generation for cooling and trapping has been described. A feedback loop is required in order to stabilise the laser. The *Red Pitaya* combines Lock-In amplifier, function generator, PID controller and oscilloscope. Therefore, the number of devices in the lab can be reduced. The digital laser lock setup has the advantage that the laser can be locked remotely and lock settings can be saved and easily reloaded. A drawback is the inconvenient *PyrPL* oscilloscope, which can not be replaced so easily, since the *Red Pitaya* has only two SMA outputs. These are already occupied providing the modulation signal and the PID control.

The potassium laser table was designed, such that it is possible to switch between the two isotopes ^{39}K and ^{40}K. This can be achieved by simply changing the RF-frequency of the offset lock and turning certain AOMs off and EOMs on. The drawback for this flexibility is that the alignment of the second double-pass for generating the repumper for ^{39}K is challenging. The (1,1) and (0,0) have to be perfectly overlapped and coupled into a single-mode fibre. In Addition to the alignment difficulties, 50% of the power is lost, since the (1,0) and (0,1) order are omitted.

4.6 SUMMARY

To generate light for trapping and cooling purposes, the following steps are needed: Light generation, frequency stabilisation, and shifting. The light is generated by commercially available diode lasers and further stabilised and shifted with MHz precision. A spectroscopy scheme and feedback system stabilises the frequency. The light is then split up into multiple paths and shifted in frequency by AOMs and EOMs. We could achieve a very stable laser lock using a *STEMlab* board and the open-source software *PyrPL*, which replaces Lock-In amplifier, function generator, PID controller and oscilloscope. On the potassium table, we aimed for a flexible setup, where we are able to switch between the isotopes ^{40}K and ^{39}K.

TWO DIMENSIONAL MAGNETO-OPTICAL TRAP

The setup for the 2D-MOT is described in this chapter. Two 2D-MOTs are built up, to separate the species at this cooling step. The setups are identical, differing only in relevant atomic parameters, e.g. oven temperature, magnetic field or coatings on optics.

5.1 ATOM PREPARATION

In order to prepare the atoms, the oven has to be filled as described in subsection 3.2.4. Next, the oven has to be heated to increase the vapour pressure in the chamber, in order to load the atoms from the background into the 2D-MOT. The ovens are heated with band heaters (*Acim Jouanin, L3420C9A5*), that are clamped to the oven.

The temperature stabilisation of the ovens, and all other temperature stabilisation tasks, are standardised using a commercially available dimmer (*NS80*) to power the heating clamps. The dimmer is controlled by a microcontroller (*Arduino*). K-type thermocouples are used to measure the temperature. The thermocouple signal is further amplified by an amplifier board (*Adafruit AD8495*). Set points and PID values can be adjusted via a flask (a Python library) based web server [43]. Connecting multiple devices via USB to one PC, resulted in compatibility issues. This is addressed by using Ethernet connections, having the following advantages: No limitations of the number of physical ports on the PC and Devices can be accessed from anywhere in the network. However, the different devices can not be powered via Ethernet, unlike USB, that requires external power supplies.

Aiming for a remotely controlled experiment, the system was updated to an Ethernet-based communication using *Arduino YUNs*, which also has the advantage that new programme versions can be uploaded without serial connection, making it possible to remotely implement a new version to any *Arduino* without having to de-assemble the specific setup.

5.2 OPTICS

The laser table and the optical table, that includes the vacuum system, were separated. The light is transferred from one table to another via polarisation-maintaining single-mode optical fibres. For a 2D-MOT, four beams are needed. Due to power constraints, the beams are set up using retro-reflectors (fig. 5.1). Therefore, light has to be split into two beams and expanded with a telescope, before passing through the cham-

ber and getting reflected by the retro-reflectors, consisting of a mirror and a quarter wave-plate to ensure the correct polarisation of the beam. In the 2D-MOT setup, silver mirrors are used, since dielectric mirrors can distort the polarisation. The beam is expanded to $\approx 10\,\text{mm}$ in diameter using a telescope with $f_1 = -2.5\,\text{mm}$ and $f_2 = 10\,\text{mm}$.

A compact setup is desired as shorter beam paths increase the stability of the 2D-MOT. Therefore, we split and expanded the beams on a breadboard, which is mounted such that the multiplexed beams (1 and 2) are directly facing the chamber (fig. 5.1 right). Mirrors, that guide the beams into the chamber, are mounted onto the supporting structure of the 2D-MOT chamber. The retro-reflectors are mounted on a flange adapter (*Thorlabs VFA275M*) with a cage system. Between the two paths is enough space to mount the optics for the push beam and a camera. Unfortunately, the flange-cage adapter and the top viewport collide. Therefore, the flange-cage adapter had to be cut as indicated in red in figure 5.1. In addition to the 2D-MOT beams, the top viewport
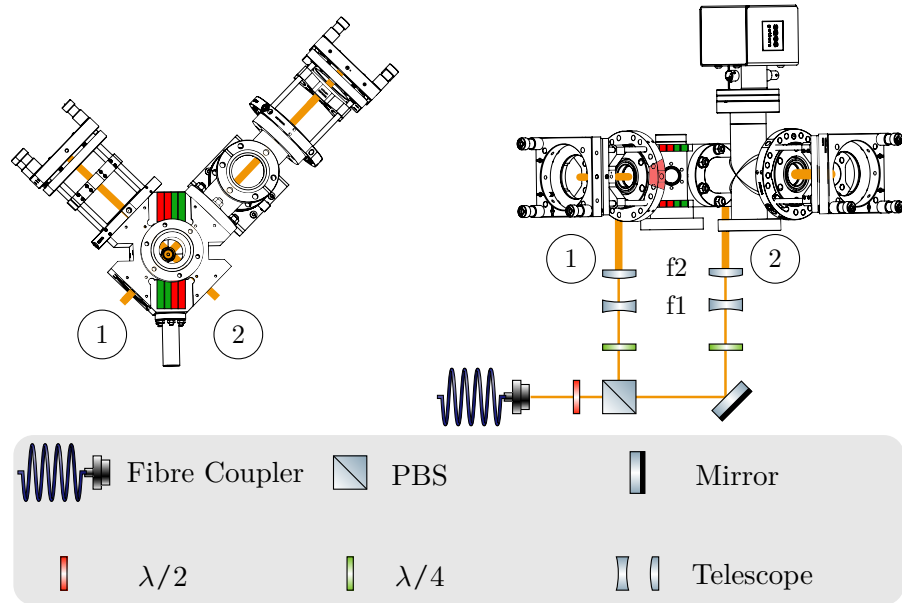
Figure 5.1: Optical setup of the 2D-MOT. Left: Front view (slightly tilted angle) of the chamber. The perpendicular 2D-MOT beams (1 and 2) are inserted through the lower viewports. The retro-reflectors are mounted directly onto the viewports. Right: Top view of the 2D-MOT optics. The light is split and expanded before it is guided into the chamber. The cut-out of the flange-cage adapter, that is necessary in order for it to be able to fit next to the viewport and band heater, is indicated in red.

can be used to implement a Zeeman Slower beam. To avoid the top viewports being blocked by depositions of atoms, it is heated with a heating clamp to $70\,^{\circ}\text{C}$ in the case of sodium.

5.3 MAGNETIC FIELD

Finally, to achieve 2D-MOT a quadrupole field is needed. Following the design of Lamporesi et al. [29] and Tiecke et al. [44], neodymium magnets (*ECLIPSE N750-RB*) were used instead of coils. These permanent magnets are affordable, space-efficient and more stable then regular coils. However, it is more complicated to change the magnetic field strength and the maximum operating temperature is 80 °C, limiting the bake-out temperature. Since the 2D-MOT acts as a pre-cooling stage, there is no need to tune the magnetic field strength during operation.

The dimensions of the magnets are $3\,\mathrm{mm}\times10\,\mathrm{mm}\times25\,\mathrm{mm}$, with the magnetic dipole oriented along the $3\,\mathrm{mm}$ axis. The magnetisation of the magnets has been measured by Lamporesi et al. to $0.65\,\mathrm{Am^2}$ [29].

Four stacks of magnets are used to generate the quadrupole field for the 2D-MOT, creating a gradient along the z-axis, which can be used for a Zeeman Slower. The positions and orientation of the magnets are indicated in figure 5.2. The magnetic dipoles are orientated along the
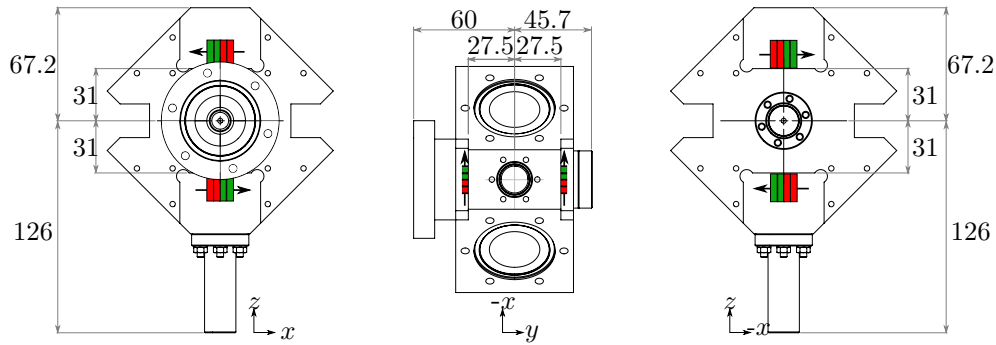
Figure 5.2: Positioning of the magnets. View in push beam direction (Left), the upper dipole is orientate to the left, and the lower one to the right, View from the top (Centre) and view against push beam direction (Right). The magnets are oriented, such that the magnetic dipoles are facing in opposite directions below and above the push beam.

x-axis, indicated by an arrow. The two stacks above the push beam are both orientated to the left, whereas the two stacks below the push beam are both oriented to the right.

For characterisation purposes, the magnetic field strength and the gradients were simulated using *Python*. The origin is set to be the centre of the 2D-MOT. The positions of the stacks of magnets are then given by $(0,\pm32.5,\pm43.5)$. A very simple model is used for the simulation: Each magnet is considered as one magnetic dipole. The magnetic field is calculated by summing up all fields created by those dipoles. The

magnetic field, resulting from one magnetic dipole, at position $\boldsymbol{r}$ is given by

$$\boldsymbol{B}(\boldsymbol{r}) = \frac{\mu_0}{4\pi} \left(\frac{3((\boldsymbol{r} - \boldsymbol{r}_0) \left[\boldsymbol{m}\, (\boldsymbol{r} - \boldsymbol{r}_0) \right]}{|\boldsymbol{r} - \boldsymbol{r}_0|^5} - \frac{\boldsymbol{m}}{|\boldsymbol{r} - \boldsymbol{r}_0|^3} \right), \qquad (5.1)$$

with the vacuum permeability μ_0. The resulting stream-plots in the xz- and yz-plane are shown in figure 5.3, where the chamber drawing is embedded in the background (note that the chamber is not included in the calculation). The xz-plane shows the necessary quadrupole field for the 2D-MOT, whereas the yz-plane shows a homogeneous field along the push beam axis. No colour-map is available for the yz-plane, since this plane is in dipole direction, leading to large values on the position of the magnets and comparably small values everywhere else. Further-
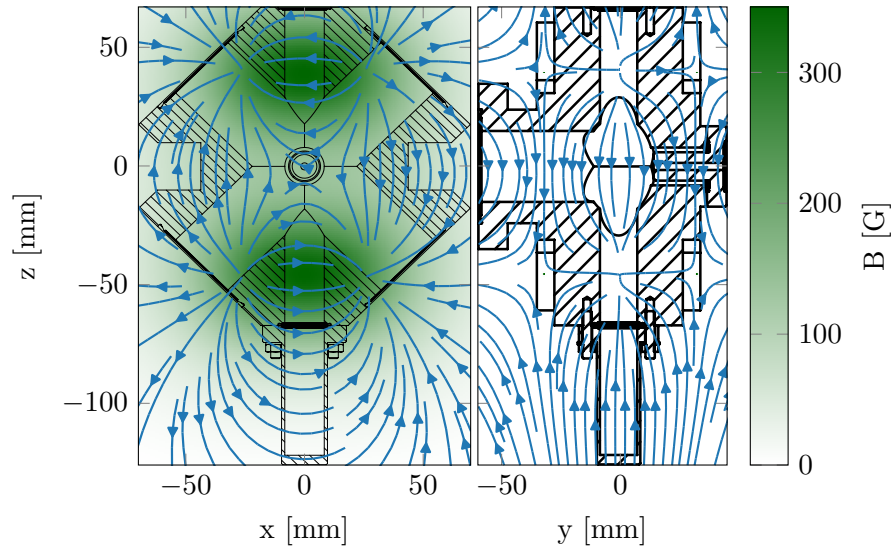
(a) Quadrupole magnetic field in the 2D-MOT beam (xz)-plane.

(b) Magnetic field in (yz)-plane.

Figure 5.3: Numerical calculation of the Na 2D-MOT magnetic field, for the xz- and yz-plane with the chamber drawing embedded into the background. The yz-plane is without colour-map, since this plane is located in the dipole.

more, the magnetic field along the 2D-MOT-beam axis and the Zeeman slower axis is calculated and shown in figure 5.4. For sodium, magnetic gradients of $60\,\mathrm{G/cm}$ are used [29, 45], which can be achieved using stacks of nine magnets. For potassium, gradients between 10 and 30 G/cm are used [45–47], which can be achieved by two to four magnets. The simulations have been verified for the case of two magnets in a stack in [36], where the magnetic field along the 2D-MOT-beam direction was measured with a Gaussmeter, using a 3d-printed model of the chamber.
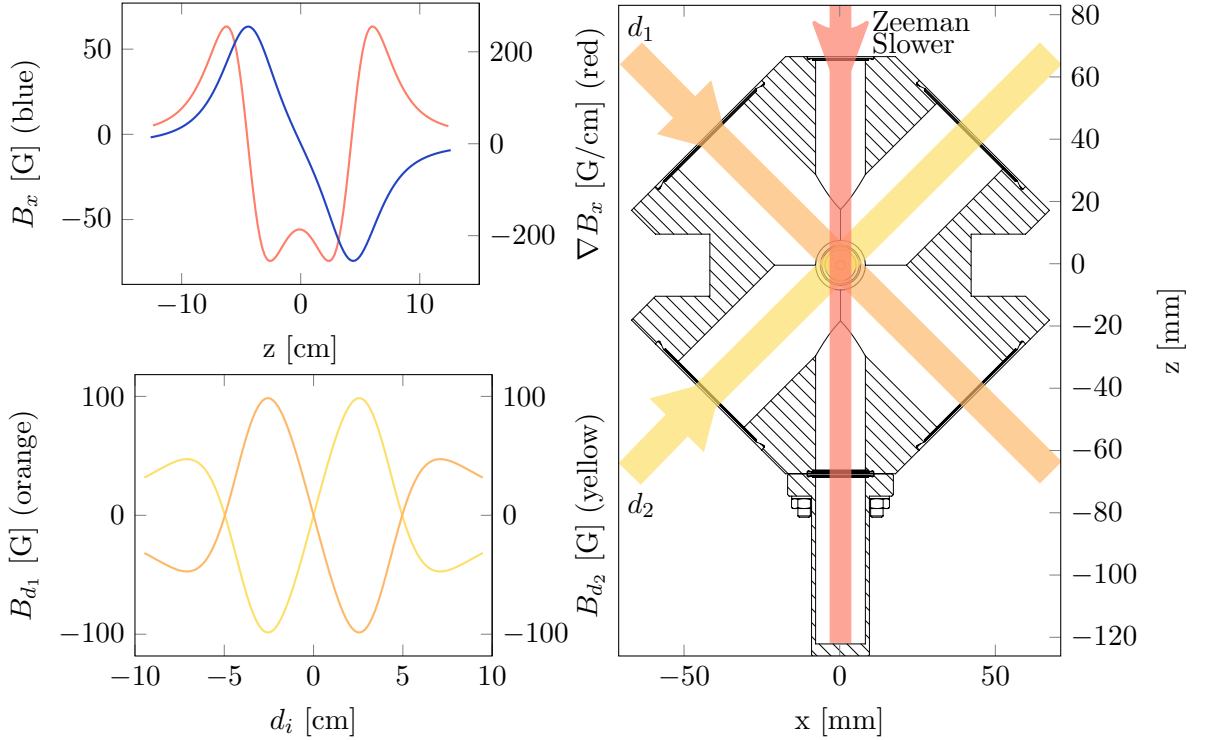
(a) Magnetic field along 2D-MOT beams and Zeeman Slower beam.

(b) 2D-MOT beams and Zeeman Slower beam in the xy-plane.

Figure 5.4: Magnetic fields along 2D-MOT beams and Zeeman Slower beam for 9 magnets per stack.

5.4 RESULTS

A CMOS camera (*Mako G-030*) with an appropriate objective is used to image the area in front of the differential pumping stage. While hunting for the 2D-MOT, a series of parameters were tuned. The alignment of the 2D-MOT beams was achieved by using paper irises, which are placed on top of the viewports. The observation of fluorescence and a stable laser lock ensured the correct frequencies. This leaves the polarisation of the beams and the magnetic field as tunable parameters. The magnets were mounted by eye to the desired position. The polarisation was checked with a polarimeter. Both beams should enter the chamber with σ_+-polarisation.

5.4.1 *Sodium*

For sodium, we were able to observe a 2D-MOT with σ_R-polarisation of the left beam (1) and σ_L-polarisation of the right beam (2). The 2D-MOT was a little bit off centred at first, which was improved by changing the position of the magnets. AOM and EOM frequencies, laser

power, and beam alignment were optimised to improve loading into the 3D-MOT. This resulted in a bigger 2D-MOT in order for it to be possible to observe the 2D-MOT by eye. Figure 5.5 a) shows the 2D-MOT looking through the front viewport (in push beam direction). One can see the fluorescence of the crossing laser beams and in front of the black circle (the 3mm aperture of the differential pumping stage) a bright cloud, the 2D-MOT. Figure 5.5 b) shows the 2D-MOT through the top viewport, where the fluorescence of the laser beams in the horizontal can be observed and the 2D-MOT as a line perpendicular to the fluorescence.
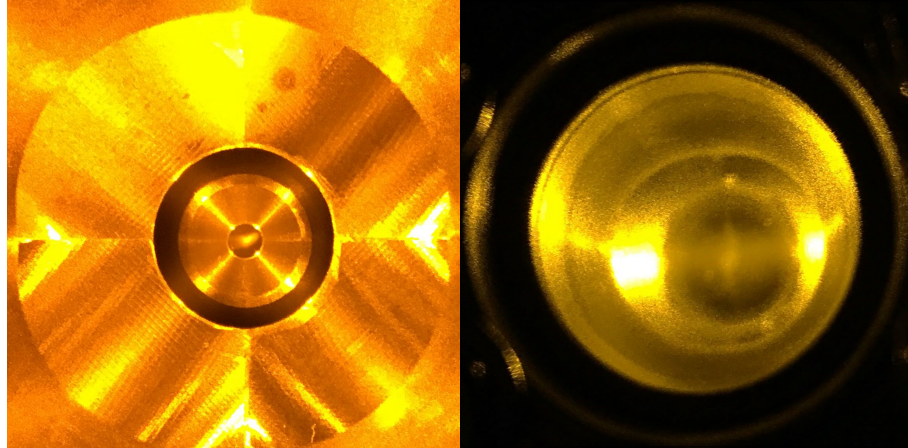
(a) 2D-MOT image from the front.   (b) 2D-MOT image from the top.

Figure 5.5: Images of the Sodium 2D-MOT. (a) Image taken from the push-beam-axis, the 2D-MOT can be identified as bright cloud in the centre. (b) Image taken from the top viewport. The 2D-MOT can be seen as very fine line orthogonal to the beam.

5.4.2 *Potassium*

For potassium, we were not able to observe a 2D-MOT. So far, two magnets per stack have been used. The fluorescence in the chamber was clearly observable. Since it was questionable, whether it is actually possible to observe the potassium 2D-MOT, we carried on setting up the 3D-MOT optics. During this time we started to get problems with the ion pump in the potassium 2D-MOT chamber, which have not been solved as of yet.

5.5 CONCLUSION

Optics and heaters are built up in a compact way, where the retro-reflectors and chamber inlet mirrors are directly mounted to the vacuum setup. Again, the compactness did lead to some space restrictions. The setup might be improved by a nipple for the Zeeman Slower view-

port, which would give more space to mount the heaters and Zeeman Slower optics directly to the chamber as it was described in section 3.3.

The temperature stabilisation circuit is standardised with commercially available modules (*Arduino Yun*, *NS80*, thermocouples), which makes it easy and fast to replace them.

As expected, the sodium 2D-MOT was observed straight forward, whereas we were not able to observe a potassium 2D-MOT. Unfortunately, we were held back with potassium due to vacuum problems. However, because of the modular setup of the vacuum system, it was still possible to work on sodium.

5.6 SUMMARY

A sufficiently high vapour pressure is required to load the 2D-MOT from the background. This is achieved by heating the oven to $70\,°C$ for potassium and $150\,°C$ for sodium. The temperature stabilisation circuits are standardised and controlled via a device control server accessing the devices, preferably via Ethernet.

Four stacks of neodymium bar magnets generate the quadrupole field to trap the atoms, but also provide a gradient along the atom flux axis, making it possible to implement a Zeeman-Slower. The atoms are cooled and trapped in the centre with four circularly-polarised red-detuned laser beams.

DUAL-SPECIES THREE DIMENSIONAL MAGNETO-OPTICAL TRAP

The next step after the 2D-MOT is the three dimensional magneto-optical trap (3D-MOT), where the two species are trapped and cooled. However, the maximum phase space density in a MOT is insufficient to exhibit quantum behaviour. A conservative trap is required to explore quantum statistics. Therefore, it is planned to load the atoms into an optical dipole trap, where they are confined by two crossing focused far red-detuned beams. For further manipulations, optical tweezers or high magnetic fields have to be implemented. This chapter describes the experimental setup of the dual-species 3D-MOT taking spatial constraints of further implementations e.g., the dipole trap into account.

6.1 OPTICS

Optical access is not only needed for the six 3D-MOT beams, but also for further implementations (dipole trap and optical tweezers) as well as for imaging. Before the optics of the 3D-MOT are described, the requirements of the different features are summarised:

> `Imaging:` The objective for imaging should be as close to the atoms as possible. Therefore, imaging from top or bottom is favourable for our setup, due to the chamber geometry.

> `3D-MOT:` Six beams are required for the 3D-MOT. The MOT beam pairs do not necessarily need to come in under an angle of 90° to each other. Using a setup with funky angles has the disadvantage, that more power is needed and the alignment will be more complicated.

> `Dipole Trap:` To confine the atoms in all directions, a crossed dipole trap is needed. Ideally the two beams intersect under an angle of 90°.

> `Optical Tweezers:` Only one focussed beam is needed for optical tweezers. This beam can be inserted through the imagine objective.

Considering those constraints, it was decided to image the atoms from below. Funky angles in the 3D-MOT setup can be avoided by inserting two MOT beams under an angle of $\pm 45°$ from the bottom into the science chamber. The third MOT beam can be inserted orthogonally on the side. Similar to the 2D-MOT setups, the MOT-beams are retro-reflected. This configuration leaves enough space for a crossed
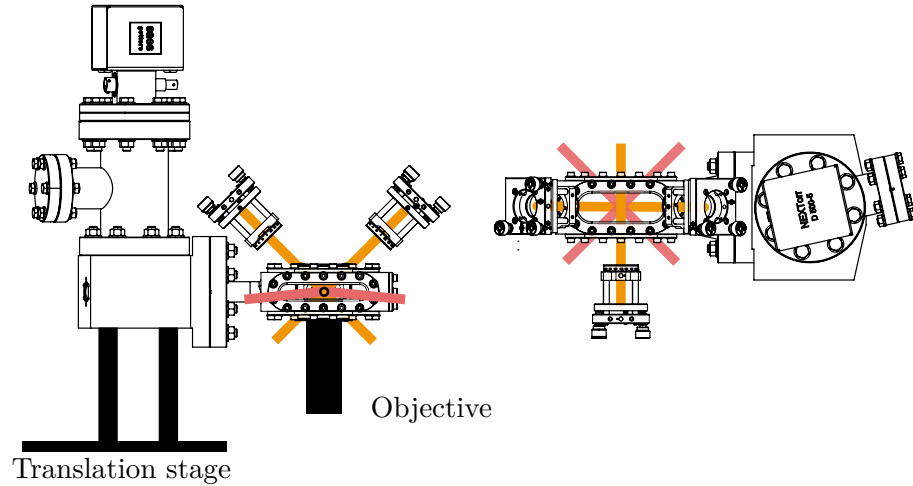
Figure 6.1: Planned optics configuration for the science chamber. The side view of the science chamber is shown on the left side, and the top view on the right. The objective is planned to be mounted from the bottom of the science chamber. Two of the MOT beams (orange) are inserted under $\pm 45\,°$ from the bottom and retro-reflected. The third MOT beam is inserted from the side. The dipole trap beams (red) are planned to be inserted under $\pm 45\,°$ through the side of the science chamber.

dipole trap in the horizontal plane, and tweezers, which do not place constraints. The planned configuration is illustrated in figure 6.1. The light for the MOT is transferred from the laser table to the optical table using polarisation-maintaining single-mode fibres. In comparison to the 2D-MOT setup, the light is first expanded to a beam diameter of 10 mm, using the fibre coupler and a collimation lens, and then split up into the three beams (A, B, and C), as illustrated in figure 6.2. The retro-reflectors for the beams, that are passing through the science chamber (A and B) under an angle of $\pm 45\,°$, are mounted above the top viewport. Therefore, the height of the optics breadboard is chosen, such that the beams can be reflected with a mirror into the science chamber. This height is limited by the rest of the vacuum system, and therefore the breadboard of the translation stage as indicated in figure 6.1. The height is chosen adequately that the mirrors can be mounted in front of the translation stage. The third MOT beam (C) is raised with a periscope. The light for both species is overlapped, using dichroic mirrors, before entering the science chamber. The retro-reflectors consist of achromatic quarter-wave plates $(400 - 800\,\text{nm})$, which are mounted to protected silver mirrors with a 30 mm cage system. The achromatic quarter-wave plate assures the correct wavelength range for both sodium, and potassium.
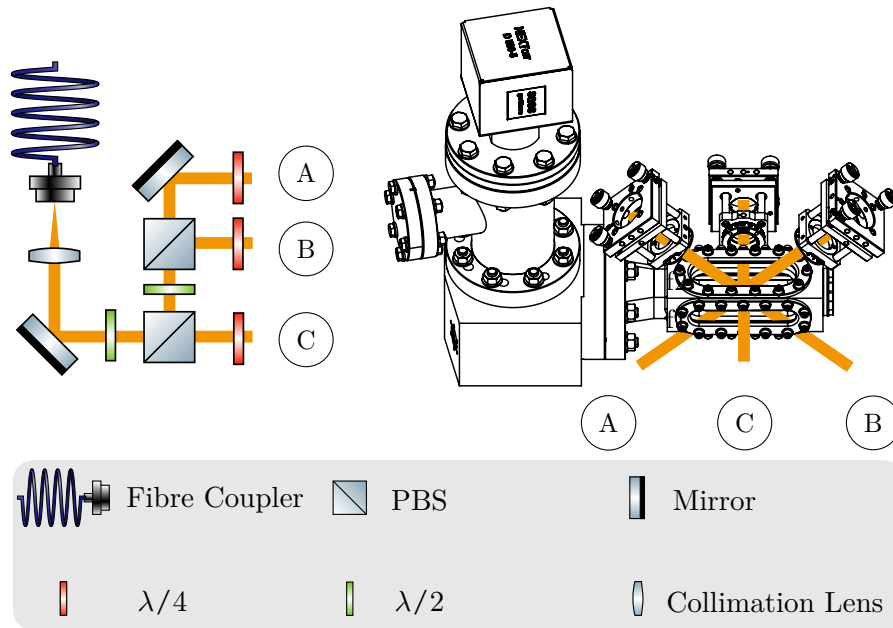
Figure 6.2: Optical setup of the 3D-MOT. (Left) Top view of the 3D-MOT optics. The light is expanded and then split into three paths A, B, and C. (Right) Slightly tilted view from the side onto the science chamber. The three MOT beams and their retro-reflectors are indicated.

6.2 MAGNETIC FIELDS

In the following listing, a short summery on the requirements of the different magnetic field coils that have to be assembled around the science chamber is given. The resulting coil configuration plan is shown in figure 6.3.

MOT coils: For the 3D-MOT a quadrupole field is needed, that can be generated by a pair of coils (gradient-field Maxwell coil). Gradients of the order of $10\,\mathrm{G/cm}$ are needed for the MOT. The beam configuration requires the coils to be mounted on the sides of the science chamber.

Feshbach coils: Inter- and intra- species interactions can be tuned using Feshbach resonances. For sodium and potassium, magnetic fields of a few hundred Gauss are needed. The creation of high magnetic fields is easiest if the coil separation of a pair of Helmholtz coils is small. Therefore, it is favourable to mount the coils along the shorter side of the science chamber.

Compensation Coils: Since the atoms are very sensitive to magnetic fields, stray magnetic fields have to be cancelled out. Consequently, three pairs of Helmholtz coils are needed, to compensate magnetic fields in all three dimensions. The compensation coils

can be large, however they should not include the magnet of the ion pump.

The compensation coils can be implemented by a set of three coils which are quite large, leaving space for retro-reflectors and other coils. However, the coils will be chosen small enough, so that the ion pump is not in the coil frame. Feshbach coils and MOT coils are often combined and switched between Helmholtz and gradient-field Maxwell configuration using an H-bridge. It is favourable for the setup to have the Feshbach coils and MOT coils oriented orthogonally to each other. Consequently, the coils are separated into two pairs of coils. This has the advantage, that they can be driven independently from each other. On the other hand, the space gets more restricted. Due to the chamber geometry of
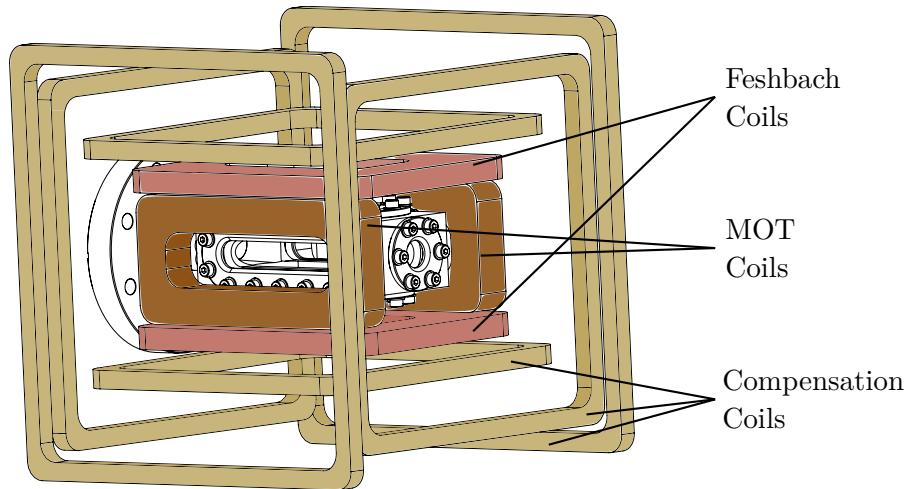
Figure 6.3: Planned configuration for the magnetic field coils. Five pairs of coils are needed: Three compensation coils, one MOT coil, and one Feshbach coil. Dimensions of the coils are not to scale. Figure adopted from [36].

the science chamber, rectangular coils are used. The MOT coils were designed so that passive cooling is sufficient. The winding process and characterisation of the MOT coils are described in [36]. The most important parameters are summarised in table 6.1. The MOT holders are made out of aluminium U-profiles, that are laser safe in contrast to plastic. However, since the coils will be turned on and off rather fast, eddy currents can be induced in the aluminium MOT frames. Therefore, the frames are cut in small parts and isolated from each other.

6.3 RESULTS

The process of hunting for the 3D-MOT is similar to the 2D-MOT case. The detunings are similar to those of the 2D-MOT, so that 2D-MOT detunings provide excellent starting values. As it was done for the 2D-MOT, the alignment was assured using paper irises. Beam polarisa-

Table 6.1: Parameters of the MOT coils. Adopted from [36].

Coil Dimension	120×30	mm
Distance between Coils	77	mm
Turns per Coil	30	
Wire Diameter	4×1	mm
Operating Current	20	A
Resistance	290	mΩ
Inductance	220	μH
Magnetic Field Gradient	15	G/cm
Maximum Operating Temperture	80	°C

tions and power balances are checked using polarimeter and powermeter respectively. The current in the coils can easily be changed and was, therefore, tuned after the polarisations were set. Indeed a sodium MOT could be observed after changing the current in the coils (fig. 6.4). A second CMOS camera with objective is used for imaging the 3D-MOT. While hunting the potassium 2D- and 3D-MOT vacuum problems occurred in the 2D-MOT chamber. Benefiting from the modular setup, this did not effect the progress with sodium.
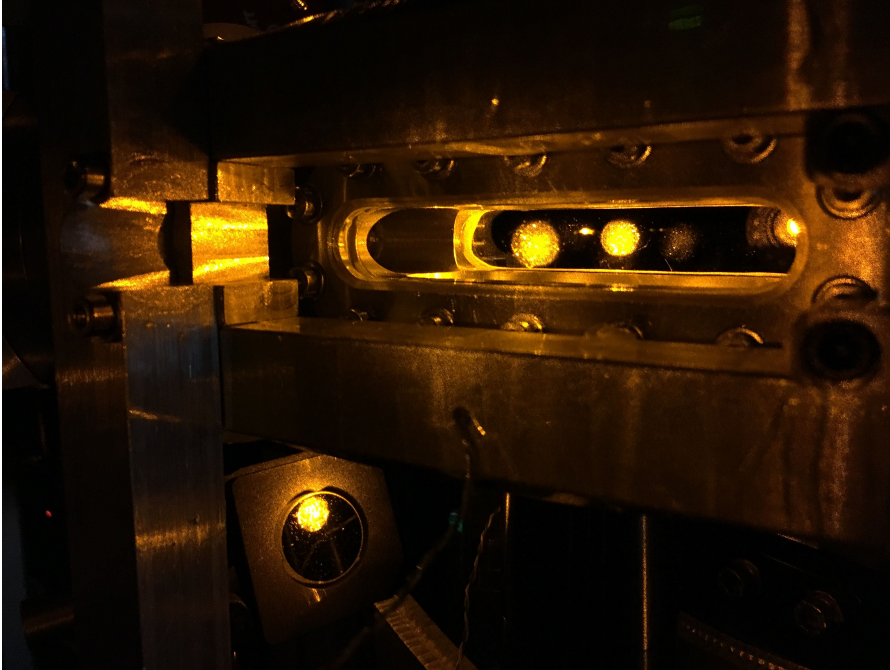
Figure 6.4: Image of the first sodium 3D-MOT. Reflections of the horizontal MOT-beam (C) passing through the glass can be seen to the left and right of the MOT.

6.4 CONCLUSION

While setting up the 3D-MOT optics, further implementations have been considered, without the need of compromises, as of yet. It was challenging to mount the mirror post of the mirror that guides beam A into the science chamber, such that it is not mounted onto the translation stage. This problem could be avoided by a cutting in the translation stage breadboard. The translation stage has proven itself helpful while mounting the coils and optics. The mutual orientation of the coils was checked by magnetic field measurements in the final position. The coil holders are constructed from aluminium, with cuttings to suppress Eddy currents. However, the science chamber itself resembles a closed conducting surface, but titanium is poorly conducting and therefore, should not be critical.

6.5 SUMMARY

The light for sodium and potassium is split independently into three beams, and then overlapped by dichroic mirrors, before passing through the science chamber. The imaging is planned to be from below. To avoid funky angles of the 3D-MOT beams, two beams are passing through the science chamber under an angle of $\pm 45\,°$ from below, while the third beam enters from the side. This leaves enough space to implement a crossed dipole trap in the future. The quadrupole field for the MOT, is generated by a gradient-field Maxwell coil pair mounted to the sides of the chamber. Furthermore, a pair of coils in Helmholtz configuration is planned above and below the science chamber for Feshbach resonances, and three pairs of Helmholtz coils to compensate stray magnetic fields. A 3D-MOT of sodium could be observed with this setup.

CONCLUSION AND OUTLOOK

This thesis describes the setup of a new ultracold sodium potassium mixture experiment, in which design decisions and the associated compromises are discussed. The focus is put on a modular, robust and compact setup. Modularity is achieved by keeping both species independent as long as possible, while building both up from the same components. A versatile laser system makes it possible to switch between ^{39}K and ^{40}K and, enables the study of Bose-Bose and Bose-Fermi mixtures. As a pre-cooling step for the dual-species three-dimensional magneto-optical trap, a two dimensional magneto-optical trap is used for each species. The resulting setup is compact enough, to be mounted on a translation stage, which offers more flexibility. The compact optical setup combined with the separation of species makes it a very robust setup, where potentially occurring problems of one species keep the other unaffected.

Considering the recent observation of a 3D-MOT of sodium atoms, the next steps include the optimisation of the MOT in terms of loading rate and atom numbers. For efficient optimisation of MOT parameters like laser detuning, magnetic field gradients, or laser powers an experimental control system has to be implemented. However, a dual-species 3D-MOT is needed, thus we will focus on solving the issues in the potassium 2D-MOT chamber, to avoid letting potassium slide behind. Further steps towards quantum degeneracy are the implementation of a dipole trap, optical tweezers, and an active magnetic field stabilisation.

Our first overreaching goal is to have a sodium Bose-Einstein condensate in a dipole trap and implement optical tweezers for single potassium atoms. Having prepared the quantum gases of both species, we would start the first line of quantitative studies by performing non-demolition thermometry experiment as suggested in a recent proposal [48]. This would also serve as a benchmark on the experiment stability.

BIBLIOGRAPHY

[1]   Immanuel Bloch, Jean Dalibard, and Sylvain Nascimbene. "Quantum simulations with ultracold quantum gases". In: *Nature Physics* 8.4 (2012), p. 267.

[2]   Richard P. Feynman. "Simulating physics with computers". In: *International Journal of Theoretical Physics* 21.6 (1982), pp. 467–488. ISSN: 1572-9575. DOI: 10.1007/BF02650179. URL: https://doi.org/10.1007/BF02650179.

[3]   Torben A. Schulze, Torsten Hartmann, Kai K. Voges, Matthias W. Gempel, Eberhard Tiemann, Alessandro Zenesini, and Silke Ospelkaus. "Feshbach spectroscopy and dual-species Bose-Einstein condensation of ^{23}Na$-^{39}$K mixtures". In: *Phys. Rev. A* 97 (2 2018), p. 023623. DOI: 10.1103/PhysRevA.97.023623. URL: https://link.aps.org/doi/10.1103/PhysRevA.97.023623.

[4]   Cheng-Hsun Wu, Jee Woo Park, Peyman Ahmadi, Sebastian Will, and Martin W. Zwierlein. "Ultracold Fermionic Feshbach Molecules of ^{23}Na^{40}**K**". In: *Phys. Rev. Lett.* 109 (8 2012), p. 085301. DOI: 10.1103/PhysRevLett.109.085301. URL: https://link.aps.org/doi/10.1103/PhysRevLett.109.085301.

[5]   Z. Hadzibabic, C. A. Stan, K. Dieckmann, S. Gupta, M. W. Zwierlein, A. Görlitz, and W. Ketterle. "Two-Species Mixture of Quantum Degenerate Bose and Fermi Gases". In: *Phys. Rev. Lett.* 88 (16 2002), p. 160401. DOI: 10.1103/PhysRevLett.88.160401. URL: https://link.aps.org/doi/10.1103/PhysRevLett.88.160401.

[6]   M. Mudrich, S. Kraft, K. Singer, R. Grimm, A. Mosk, and M. Weidemüller. "Sympathetic Cooling with Two Atomic Species in an Optical Trap". In: *Phys. Rev. Lett.* 88 (25 2002), p. 253001. DOI: 10.1103/PhysRevLett.88.253001. URL: https://link.aps.org/doi/10.1103/PhysRevLett.88.253001.

[7]   G. Modugno, G. Ferrari, G. Roati, R. J. Brecha, A. Simoni, and M. Inguscio. "Bose-Einstein Condensation of Potassium Atoms by Sympathetic Cooling". In: *Science* 294.5545 (2001), pp. 1320–1322. DOI: 10.1126/science.1066687. URL: https://science.sciencemag.org/content/294/5545/1320.

[8]   Wolfgang Niedenzu, Igor Mazets, Gershon Kurizki, and Fred Jendrzejewski. "Quantized refrigerator for an atomic cloud". In: *arXiv e-prints* (2019). DOI: arXiv:1812.08474v2. URL: https://arxiv.org/abs/1812.08474v2.

[9]   Fred Jendrzejewski. *Short notes on the Kondo effect and its potential realization in ultracold atomic gases.* In: Authorea, accessed June 2019. URL: https://www.authorea.com/users/143341/articles/203821-short-notes-on-the-kondo-effect-and-its-potential-realization-in-ultracold-atomic-gases.

[10]   Jinhong Park, S.-S. B. Lee, Yuval Oreg, and H.-S. Sim. "How to Directly Measure a Kondo Cloud's Length". In: *Phys. Rev. Lett.* 110 (24 2013), p. 246603. DOI: 10.1103/PhysRevLett.110.246603. URL: https://link.aps.org/doi/10.1103/PhysRevLett.110.246603.

[11]   Johannes Bauer, Christophe Salomon, and Eugene Demler. "Realizing a Kondo-Correlated State with Ultracold Atoms". In: *Phys. Rev. Lett.* 111 (21 2013), p. 215304. DOI: 10.1103/PhysRevLett.111.215304. URL: https://link.aps.org/doi/10.1103/PhysRevLett.111.215304.

[12]   V Kasper, F Hebenstreit, F Jendrzejewski, M K Oberthaler, and J Berges. "Implementing quantum electrodynamics with ultracold atomic systems". In: *New Journal of Physics* 19.2 (2017), p. 023030. DOI: 10.1088/1367-2630/aa54e0. URL: https://doi.org/10.1088%2F1367-2630%2Faa54e0.

[13]   U.-J. Wiese. "Ultracold quantum gases and lattice systems: quantum simulation of lattice gauge theories". In: *Annalen der Physik* 525.10-11 (), pp. 777–796. DOI: 10.1002/andp.201300104. URL: https://onlinelibrary.wiley.com/doi/abs/10.1002/andp.201300104.

[14]   M. Dalmonte and S. Montangero. "Lattice gauge theory simulations in the quantum information era". In: *Contemporary Physics* 57.3 (2016), pp. 388–412. DOI: 10.1080/00107514.2016.1151199. URL: https://doi.org/10.1080/00107514.2016.1151199.

[15]   Erez Zohar, J. Ignacio Cirac, and Benni Reznik. "Quantum simulations of gauge theories with ultracold atoms: Local gauge invariance from angular-momentum conservation". In: *Phys. Rev. A* 88 (2 2013), p. 023617. DOI: 10.1103/PhysRevA.88.023617. URL: https://link.aps.org/doi/10.1103/PhysRevA.88.023617.

[16]   T. V. Zache, F. Hebenstreit, F. Jendrzejewski, M. K. Oberthaler, J. Berges, and P. Hauke. "Quantum simulation of lattice gauge theories using Wilson fermions". In: *Quantum Science and Technology* 3.3 (2018), p. 034010. DOI: 10.1088/2058-9565/aac33b. URL: https://doi.org/10.1088%2F2058-9565%2Faac33b.

[17]   C.J. Foot and D.P.C.J. Foot. *Atomic Physics.* Oxford Master Series in Physics. OUP Oxford, 2005. ISBN: 9780198506959.

[18]   Jan Krieger. "Zeeman-Slower und Experimentsteuerung für das NaLi-Experiment". Diplom Thesis. University of Heidelberg, 2008.

[19]   Steven Chu. "Nobel Lecture: The manipulation of neutral particles". In: *Rev. Mod. Phys.* 70 (3 1998), pp. 685–706. DOI: `10.1103/RevModPhys.70.685`. URL: `https://link.aps.org/doi/10.1103/RevModPhys.70.685`.

[20]   Claude N. Cohen-Tannoudji. "Nobel Lecture: Manipulating atoms with photons". In: *Rev. Mod. Phys.* 70 (3 1998), pp. 707–719. DOI: `10.1103/RevModPhys.70.707`. URL: `https://link.aps.org/doi/10.1103/RevModPhys.70.707`.

[21]   William D. Phillips. "Nobel Lecture: Laser cooling and trapping of neutral atoms". In: *Rev. Mod. Phys.* 70 (3 1998), pp. 721–741. DOI: `10.1103/RevModPhys.70.721`. URL: `https://link.aps.org/doi/10.1103/RevModPhys.70.721`.

[22]   W. D. Phillips and H. J. Metcalf. "Cooling and trapping atoms". In: *Scientific American* 256 (Mar. 1987), pp. 50–56. DOI: `10.1038/scientificamerican0387-50`.

[23]   P. J. Ungar, D. S. Weiss, E. Riis, and Steven Chu. "Optical molasses and multilevel atoms: theory". In: *J. Opt. Soc. Am. B* 6.11 (1989), pp. 2058–2071. DOI: `10.1364/JOSAB.6.002058`. URL: `http://josab.osa.org/abstract.cfm?URI=josab-6-11-2058`.

[24]   Claude N. Cohen-Tannoudji and William D. Phillips. "New Mechanisms for Laser Cooling". In: *Physics Today* 43.10 (1990), pp. 33–40. DOI: `10.1063/1.881239`. URL: `https://doi.org/10.1063/1.881239`.

[25]   Pfeiffer Vacuum GmbH. *The Vacuum Technology Book*. Vol. Volume 1. 2008.

[26]   J.H. Moore, C.C. Davis, M.A. Coplan, and S.C. Greer. *Building Scientific Apparatus*. Cambridge University Press, 2009. ISBN: 9781139478656.

[27]   E Pedrozo-Peñafiel, F Vivanco, P Castilho, R R Paiva, K M Farias, and V S Bagnato. "Direct comparison between a two-dimensional magneto-optical trap and a Zeeman slower as sources of cold sodium atoms". In: *Laser Physics Letters* 13.6 (2016), p. 065501. DOI: `10.1088/1612-2011/13/6/065501`. URL: `https://doi.org/10.1088%2F1612-2011%2F13%2F6%2F065501`.

[28]   Oerlikon Leybold Vacuum. "Fundamentals of Vacuum Technology, 00.200. 02, Kat". In: *Nr* 199 (2007).

[29]   G. Lamporesi, S. Donadello, S. Serafini, and G. Ferrari. "Compact high-flux source of cold sodium atoms". In: *Review of Scientific Instruments* 84.6 (2013), p. 063102. DOI: `10.1063/1.4808375`. URL: `https://doi.org/10.1063/1.4808375`.

[30]   Alexander Baumgärtner. "A new apparatus for trapping and manipulating single Strontium atoms". Master Thesis. California Insitute of Technology, 2017.

[31] K. Jousten and C.B. Nakhosteen. *Handbook of Vacuum Technology*. Wiley, 2016. ISBN: 9783527688258. URL: https://books.google.de/books?id=EbxlDAAAQBAJ.

[32] J.J. Bozzola and L.D. Russell. *Electron Microscopy: Principles and Techniques for Biologists*. Jones and Bartlett series in biology. Jones and Bartlett, 1999. ISBN: 9780763701925. URL: https://books.google.de/books?id=zMkBAPACbEkC.

[33] Gamma Vacuum. *Ion Pump Operation*. accessed 17 June 2019. URL: https://www.gammavacuum.com/index.php/theory-of-operation/.

[34] TOPTICA Photonics AG. *Tunable Diode Lasers*. accessed 17 June 2019. URL: https://www.toptica.com/fileadmin/Editors_English/11_brochures_datasheets/01_brochures/toptica_BR_Scientific_Lasers.pdf.

[35] Florian Volker Nicolai. "Design and construction of a fiber-coupled tapered amplifier system". Master Thesis. University of Heidelberg, 2017.

[36] Jan Kilinc. "Starting a Na-K experiment for simulating quantum many-body phenomena". Master Thesis. University of Heidelberg, 2019.

[37] Tobias Gerard Tiecke. "Feshbach resonances in ultracold mixtures of the fermionic quantum gases 6Li and 40K". PhD thesis. University of Amsterdam, 2009.

[38] Daniel A. Steck. "Sodium D Line Data". Dec. 2010. URL: http://steck.us/alkalidata.

[39] R. Scholten. *Lock-in amplifiers*. accessed 17 June 2019. URL: http://electronics.physics.helsinki.fi/wp-content/uploads/2011/02/lockin_rob_web.pdf.

[40] E. A. Donley, T. P. Heavner, F. Levi, M. O. Tataw, and S. R. Jefferts. "Double-pass acousto-optic modulator system". In: *Review of Scientific Instruments* 76.6 (2005), p. 063112. DOI: 10.1063/1.1930095. URL: https://doi.org/10.1063/1.1930095.

[41] B.E.A. Saleh and M.C. Teich. *Fundamentals of Photonics*. Wiley Series in Pure and Applied Optics. Wiley, 2019. ISBN: 9781118770092.

[42] B. Kuhlow. "7.1 Modulators". In: *Laser Fundamentals. Part 2*. Ed. by H. Weber, G. Herziger, and R. Poprawe. Berlin, Heidelberg: Springer Berlin Heidelberg, 2006, pp. 85–110. ISBN: 978-3-540-47008-3.

[43] Fred Jendrzejewski. *Device Control Server*. GitHub repository, accessed 17 June 2019. URL: https://github.com/synqs/DeviceControlServer.

[44] T. G. Tiecke, S. D. Gensemer, A. Ludewig, and J. T. M. Walraven. "High-flux two-dimensional magneto-optical-trap source for cold lithium atoms". In: *Phys. Rev. A* 80 (1 2009), p. 013409. DOI: 10.1103/PhysRevA.80.013409. URL: https://link.aps.org/doi/10.1103/PhysRevA.80.013409.

[45] PCM Castilho, E Pedrozo-Peñafiel, EM Gutierrez, PL Mazo, G Roati, KM Farias, and VS Bagnato. "A compact experimental machine for studying tunable Bose–Bose superfluid mixtures". In: *Laser Physics Letters* 16.3 (2019), p. 035501.

[46] J. Catani, P. Maioli, L. De Sarlo, F. Minardi, and M. Inguscio. "Intense slow beams of bosonic potassium isotopes". In: *Phys. Rev. A* 73 (3 2006), p. 033415. DOI: 10.1103/PhysRevA.73.033415. URL: https://link.aps.org/doi/10.1103/PhysRevA.73.033415.

[47] Thomas Uehlinger. "A 2D Magneto-Optical Trap as a High-Flux Source of Cold Potassium Atoms". Diploma Thesis. Swiss Federal Institute of Technology Zurich, 2008.

[48] Mohammad Mehboudi, Aniello Lampo, Christos Charalambous, Luis A. Correa, Miguel Ángel García-March, and Maciej Lewenstein. "Using Polarons for sub-nK Quantum Nondemolition Thermometry in a Bose-Einstein Condensate". In: *Phys. Rev. Lett.* 122 (3 2019), p. 030403. DOI: 10.1103/PhysRevLett.122.030403. URL: https://link.aps.org/doi/10.1103/PhysRevLett.122.030403.

ACKNOWLEDGEMENTS

ERKLÄRUNG

Ich versichere, dass ich diese Arbeit selbstständig verfasst und keine anderen als die angegebenen Quellen und Hilfsmittel benutzt habe.

Heidelberg, den 17. Juni, 2019

_____

Lilo Höcker